Carbon Dioxide and Methane Emissions from a Temperate Salt Marsh Tidal Creek

Branimir Trifunovic[1], Alma Vázquez-Lule[1], Margaret Capooci[2], Angelia Lyn Seyfferth[1], Carlos Moffat[1], and Rodrigo Vargas[1]

[1]University of Delaware
[2]University of Delawarere

November 23, 2022

Abstract

Coastal salt marshes store large amounts of carbon but the magnitude and patterns of greenhouse gas (GHG; i.e., carbon dioxide (CO) and methane (CH)) fluxes are unclear. Information about GHG fluxes from these ecosystems comes from studies of sediments or at the ecosystem-scale (eddy covariance) but fluxes from tidal creeks are unknown. We measured GHG concentrations in water, water quality, meteorology, sediment CO efflux, ecosystem-scale GHG fluxes, and plant phenology; all at half-hour time-steps over one year. Manual creek GHG flux measurements were used to calculate gas transfer velocity () and parameterize a model of water-to-atmosphere GHG fluxes. The creek was a source of GHGs to the atmosphere where tidal patterns controlled diel variability. Dissolved oxygen and wind speed were negatively correlated with creek CH efflux. Despite lacking a seasonal pattern, creek CO efflux was correlated with drivers such as turbidity across phenological phases. Overall, night-time creek CO efflux (3.6 ± 0.63 µmol/m/s) was over two times higher than night-time marsh sediment CO efflux (1.5 ± 1.23 µmol/m/s). Creek CH efflux (17.5 ± 6.9 nmol/m/s) was four times lower than ecosystem-scale CH fluxes (68.1 ± 52.3 nmol/m/s) across the year. These results suggest that tidal creeks are potential hotspots for CO emissions and could contribute to lateral transport of CH to the coastal ocean due to supersaturation of CH (>6000 µmol/mol) in water This study provides insights for modelling GHG efflux from tidal creeks and suggests that changes in tide stage overshadow water temperature in determining magnitudes of fluxes.

Posted on 23 Nov 2022 — CC-BY 4.0 — https://doi.org/10.1002/essoar.10504497.1 — This a preprint and has not been peer reviewed. Data may be preliminary.

Carbon Dioxide and Methane Emissions from a Temperate Salt Marsh Tidal Creek

Authors:

Branimir Trifunovic[1], Alma Vázquez-Lule[1], Margaret Capooci[1], Angelia L. Seyfferth[1], Carlos Moffat[2], Rodrigo Vargas[1*]

Affiliations:

[1]Department of Plant and Soil Sciences, College of Agriculture & Natural Resources, University of Delaware, Newark, Delaware, USA

[2]School of Marine Science and Policy, College of Earth, Ocean, & Environment, University of Delaware, Newark, Delaware, USA

*Corresponding author: Rodrigo Vargas (rvargas@udel.edu)

Key Points:

- A creek was a hotspot for CO_2 efflux compared to the surrounding landscape
- Changes in tide stage, not water temperature variability, regulated diel creek CO_2 and CH_4 efflux
- The relative influence of non-tidal drivers of creek CO_2 and CH_4 efflux varied by plant phenological phases

Abstract

Coastal salt marshes store large amounts of carbon but the magnitude and patterns of greenhouse gas (GHG; i.e., carbon dioxide (CO_2) and methane (CH_4)) fluxes are unclear. Information about GHG fluxes from these ecosystems comes from studies of sediments or at the ecosystem-scale (eddy covariance) but fluxes from tidal creeks are unknown. We measured GHG concentrations in water, water quality, meteorology, sediment CO_2 efflux, ecosystem-scale GHG fluxes, and plant phenology; all at half-hour time-steps over one year. Manual creek GHG flux measurements were used to calculate gas transfer velocity (*k*) and parameterize a model of water-to-atmosphere GHG fluxes. The creek was a source of GHGs to the atmosphere where tidal patterns controlled diel variability. Dissolved oxygen and wind speed were negatively correlated with creek CH_4 efflux. Despite lacking a seasonal pattern, creek CO_2 efflux was correlated with drivers such as turbidity across phenological phases. Overall, night-time creek CO_2 efflux (3.6 ± 0.63 μmol/m^2/s) was over two times higher than night-time marsh sediment CO_2 efflux (1.5 ± 1.23 μmol/m^2/s). Creek CH_4 efflux (17.5 ± 6.9 nmol/m^2/s) was four times lower than ecosystem-scale CH_4 fluxes (68.1 ± 52.3 nmol/m^2/s) across the year. These results suggest that tidal creeks are potential hotspots for CO_2 emissions and could contribute to lateral transport of CH_4 to the coastal ocean due to supersaturation of CH_4 (>6000 μmol/mol) in water. This study provides insights for modelling GHG efflux from tidal creeks and suggests that changes in tide stage overshadow water temperature in determining magnitudes of fluxes.

Keywords: Carbon dioxide, methane, automated measurements, estuary, tidal channel, air-water efflux

Index Terms: 0428 Carbon cycling (4806), 0438 Diel, seasonal, and annual cycles (4227), 0442 Estuarine and nearshore processes (4235), 0497 Wetlands (1890), 3322 Land/atmosphere interactions (1218, 1631, 1843, 4301)

1 Introduction

Coastal salt marshes are becoming increasingly of interest to carbon cycle science due to the large amounts of carbon sequestered in their sediments (Howard et al., 2017). These systems are disproportionately important to the global carbon cycle relative to their small global area (22,000-400,000 km^2); on average they store 10 times more carbon per unit area than terrestrial forests (McLeod et al., 2011). However, stored carbon is vulnerable to increased erosion and decomposition due to sea level rise (Jones et al., 2018; Ruiz-Fernández et al., 2018), habitat disturbance from land cover change and seagrass accumulation, (Macreadie et al., 2013; Pendleton et al., 2012), and increased heterotrophic respiration due to rising temperatures (Bond-Lamberty et al., 2018; Kirwan et al., 2014). The vulnerability of these large carbon stocks requires detailed research into the magnitudes, patterns, and drivers of carbon exchange across different landscape features in salt marshes.

Coastal salt marshes are hotspots for carbon storage because they are sub-to-anoxic, which decreases the rate of heterotrophic decomposition of soil organic carbon (SOC). In wet sediments, limited oxygen supply drives anaerobic metabolism by soil microbes, which lowers CO_2 emissions compared to upland terrestrial environments where aerobic metabolism dominates (Greenwood, 1961; Raich & Schlesinger, 1992). Moreover, sulfate-reducing bacteria compete with methanogens for substrate, thereby lowering CH_4 production (Tobias & Neubauer, 2009). The slow rate of carbon oxidation in marsh sediments thus results in large accumulations of SOC within these ecosystems (Chmura et al., 2003). However, there is a delicate balance between anaerobic and aerobic conditions in these tidal systems due to the tidal ebb and flood, which changes the redox conditions of the sediments near tidal channels (Baumann et al., 2015). These dynamic conditions could promote emissions of CO_2 and CH_4 from the land surface and

74 water-to-atmosphere via changes in oxygen concentrations and redox oscillations (Moseman-
75 Valtierra 2012). Therefore, understanding the patterns and drivers of salt marsh greenhouse gas
76 (GHG; i.e., CO_2 and CH_4) efflux is important to understand how SOC in salt marshes will
77 respond to weather variability and global environmental change.

78 The majority of salt marsh GHG efflux studies have focused on soils/sediment (Chmura
79 et al., 2011, 2016; Tong et al., 2010, 2013; Capooci et al., 2019) or used eddy covariance towers
80 at ecosystem-scale (Forbrich et al., 2015, 2018; Moffett et al., 2010), but the dynamics of GHG
81 efflux from tidal creeks are currently unknown. Past studies on soil GHG fluxes revealed that
82 tidal patterns play an important role in GHG dynamics in these ecosystems. These tidal patterns
83 affect both CO_2 (Huertas et al., 2017) and CH_4 emissions (Tong et al., 2010) by increasing the
84 aerobic zone in the sediment profile near tidal creeks with the ebbing tide and decreasing the
85 aerobic zone with the flooding tide. Tides also affect the conditions for GHG efflux by moving
86 sediments, organic matter, and nutrients into and out of the marsh (Fagherazzi et al., 2013).
87 Despite the knowledge of tides as an important GHG efflux control, to our knowledge there have
88 been no studies of GHG efflux directly from marsh tidal channels or creeks. These landscape
89 features have been shown to be important sources of dissolved inorganic carbon to estuaries
90 (Neubauer & Anderson, 2003; Wang & Cai, 2004; Wang et al., 2016), and may be important
91 contributors of CH_4 and CO_2 efflux in marsh ecosystems.

92 Previous studies on GHG efflux from terrestrial streams, mangrove tidal creeks, and
93 coastal rivers found that flowing waters have high GHG efflux and suggest that GHG efflux
94 from salt marsh creeks could be higher per unit area than the surrounding landscape (Call et al.,
95 2015; Lauerwald et al. 2015; Linto et al., 2014; Raymond et al., 2013; Yang et al., 2017).
96 Therefore, our overarching goal was to characterize the temporal dynamics and magnitudes of

CO_2 and CH_4 efflux from a temperate salt marsh tidal creek. In particular, we aimed to a) measure the temporal patterns and magnitudes of CO_2 and CH_4 efflux from a salt marsh creek; b) identify the biophysical drivers for CO_2 and CH_4 efflux throughout the year; and c) determine how the magnitudes of CO_2 and CH_4 efflux compare to those from sediments and at the ecosystem-scale.

We explored four interrelated hypotheses: First, we hypothesized that creek GHG emissions would be higher in the summer due to the temperature dependence of heterotrophic respiration (Zhong et al., 2013) and methanogenesis (Yvon-Durocher et al., 2014). Second, water-to-atmosphere GHG efflux would be highest during ebb and flood tides as the water is moving faster than compared to the low flows at high and low tides. This hypothesis is supported by the fact that faster water velocity usually has a higher gas transfer velocity (Raymond et al., 2012). Third, dissolved oxygen and salinity are likely negative controls on CH_4 emissions due to their inhibiting effect on methanogenesis (Poffenbarger et al., 2011; Tobias & Neubauer, 2009). Fourth, the creek's CO_2 emissions (per unit area) could be higher than the surrounding soil emissions because of the high GHG efflux potential of flowing waters (Lauerwald et al., 2015; Linto et al., 2014). We addressed this research by taking advantage of automated measurements of CO_2 and CH_4 concentrations (alongside a wide array of ancillary information) which provided unprecedented information about temporal patterns of GHG emissions in tidal salt marshes.

2 Materials and Methods

2.1 Study Site

This study was carried out in the St. Jones Reserve, a component of the Delaware National Estuarine Research Reserve in Dover, Delaware, U.S.A. The study site is part of the

AmeriFlux (site ID: US-StJ) and Phenocam (site ID: stjones) networks. The GHG concentration and efflux sampling location was located at Aspen Landing within a microtidal (mean tide range of 1.5 m), mesohaline (typical salinity of 5-18 ppt) salt marsh (Delaware Department of Natural Resources and Environmental Control, 2006) tidal creek. The creek makes up 6.9% of the area of the study site (Supplementary Figure 1). *Spartina alterniflora* is the dominant plant species, making up 62.2% of the marsh's land cover with the invasive *Phragmites australis* representing 13.4% (Delaware Department of Natural Resources and Environmental Control, 2006). The reserve is located on the Atlantic Coastal Plain geologic unit (DNREC, 2006) and made up of 40% Transquaking and 40% Mispillon soils consisting of layers of mucky peat, muck, mucky silt loam, and silt loam (Soil Survey Staff, 2019). The climate is temperate with four distinct seasons and an average maximum July temperature of 31.7 °C and an average minimum January temperature of 4.4 °C (Delaware Department of Natural Resources and Environmental Control, 2006). Average precipitation is 117 cm/yr with an average snowfall of 40 cm/year (Delaware Department of Natural Resources and Environmental Control, 2006).

2.2 Plant Phenological Stages

The phenological stages were identified using the greenness index (GI), a vegetation index derived from a time lapse of Red, Green and Blue (i.e., RGB) photographs of vegetation cover that quantifies the number of green pixels relative to the overall brightness (Gillespie et al., 1987). Data were divided by phenophase as plant phenology determines primary productivity of terrestrial ecosystems (Flanagan, 2009; Richardson et al., 2010; Wu et al., 2013), and influences fluxes of dissolved organic carbon between salt marsh sediments and the water column (Dausse et al., 2011). The study site follows the PhenoCam network's protocol for data collection, storage

and processing (Seyednasrollah et al., 2019). A NetCam SC camera (StarDot Technologies, Buena Vista, CA, USA) took RGB photographs every half hour, and we identified a region of interest (ROI) adjacent to the creek. The ROI was represented mainly by *S. cynosuroides* with some *S. alterniflora*. Phenocam data were analyzed from March 3rd, 2017 to December 13th, 2017. Phenology data were revised, analyzed, and divided into phenophases using the Phenopix R package (Filippa et al., 2016). Data revision consisted of calculating the daily averages of the greenness index and filtering out images that were too dark. Four distinct phenophases were identified based on the greenness index: a) *Dormant* for when the plants were inactive during winter; b) *Greenup* for when the plants were initially growing following the *Dormant* phenophase; c) *Maturity* for when the plants reached a peak in greenness; and d) *Senescence* for when the plants started losing greenness as they moved into the *Dormant* phenophase.

2.3 Creek CO_2 and CH_4 Fluxes

The concentrations of CO_2 (pCO_2) and CH_4 (pCH_4) within the water of the creek were measured from March 3rd, 2017 to December 13th, 2017. We used an eosGP CO_2 Concentration Probe (Eosense, Dartmouth, NS, Canada) with a calibration range of 0-20,000 µmol/mol, an equilibration time of < 90 seconds, and an accuracy of +/- 200 µmol/mol, and a Mini-Pro CH_4 Probe (Pro Oceanus, Bridgewater, NS, Canada) with a calibration range of 0-10,000 µmol/mol, an equilibration time of four minutes, and an accuracy of +/- 200 µmol/mol. Data were collected every minute, corrected for changes in pressure and temperature, and averaged into 30-minute intervals. Probes were cleaned with deionized water every two weeks to prevent sediment accumulation and biofilm build-up in the sensor membranes.

Manual measurements of CO_2 and CH_4 efflux from the creek were taken every two weeks from September 2017 to December 2017 along with four 24-hour sampling campaigns (two neap tides; 9/1/17, 11/9/17, two spring tides; 9/18/17, 11/3/17) to capture tidal diel patterns. Each campaign sampled over the course of two tidal cycles, with measurements at low, flood, high, and ebb tide, for a total of eight measurements. Low tide was defined as the half-hour before and after the local minima of the water level, while high tide used the local maxima. Each local minima and maxima were calculated using the Tides package in R (Cox & Schepers, 2017). Flood tide was assigned to all measurements taken after low tide but before high tide, and ebb tide was assigned to all measurements taken after high tide but before low tide. Low tide ranged from -0.26 to -0.16 meters above sea level, flood and ebb tide ranged from -0.16 to 0.665 meters above sea level, and high tide ranged from 0.665 to 1.16 meters above sea level.

A closed-system floating flux chamber (20 cm in diameter; Rawitch, 2016) was coupled with an Ultraportable Greenhouse Gas Analyzer (Los Gatos Research, Santa Clara, CA, USA) with a range and error of 1–20,000 ± 0.3 ppm for CO_2 and 0.01–100 ± 0.002 ppm for CH_4 for flux measurements. Each manual measurement lasted 3 minutes to allow the gases to accumulate and the change in concentration within the chamber was recorded every two seconds. Creek GHG effluxes were calculated with a linear equation using the change in gas concentration over time, chamber volume and area, atmospheric pressure, water temperature, and the ideal gas law constant as described in previous studies (Pearson et al., 2016; Warner et al., 2017). Three consecutive manual measurements were taken and averaged to represent one measurement in time for subsequent analyses. A total of 38 averaged measurements were recorded and included in the final model calibration.

188 2.4 Water-to-Atmosphere Flux Model

189 Automatic concentrations and manual flux measurements of each GHG were used with
190 Equations 1 and 2 (Van Dam et al., 2019; Wanninkhof 2014) to build a model of water-to-
191 atmosphere GHG efflux from the tidal creek. First, the gas transfer velocity was calculated as:

192 $$\boldsymbol{k} = \frac{\boldsymbol{fGas(measured)}}{\boldsymbol{\Delta pGas * k_0}} \quad \text{(Equation 1)}$$

193

194 where *k* is the gas transfer velocity (m/s), *ΔpGas* is the difference between the concentrations of
195 the GHG of interest in the water and the atmosphere (µmol/mol), k_0 is the solubility coefficient
196 of the GHG of interest (mol/L/atm), and *fGas(measured)* is the measured flux (from manual
197 measurements) of the GHG of interest (µmol/m^2/s). For each GHG, a *k* was calculated for each
198 of the four tide stages using the mean of all measurements taken at each tide stage. Then
199 *fGas(modelled)*, representing the predicted GHG efflux (µmol/m^2/s), was calculated as:

200

201 $$\boldsymbol{fGas(modelled) = k * k_0 * \Delta pGas} \quad \text{(Equation 2)}$$

202

203 where *k* is the gas transfer velocity for a specific tidal stage, and *ΔpGas* is the difference between
204 the concentrations of the GHG of interest in the water and the concentration of the GHG in the
205 atmosphere for a specific tidal stage (associated with the respective *k*). Site-specific *k* values
206 were used for the gas flux model calculation but standardized k_{600} values were calculated for
207 easier comparison with other gas transfer studies using Equation 3 with n as 0.5 (Lorke et al.,
208 2015) and a temperature and salinity dependent Schmidt number (Sc; Wanninkhof 2014):

209 $$\boldsymbol{k_{600} = k * \frac{600^{-n}}{Sc}} \quad \text{(Equation 3)}$$

210

211 2.5 Ancillary Measurements

212 Ecosystem-scale CO_2 and CH_4 fluxes were measured by the Eddy Covariance (EC)
213 technique. The EC tower is equipped with a WindMaster Pro anemometer, model 160724 (Gill
214 Instruments, Lymington, Hamisphere, UK), a LI-7200RS enclosed path CO_2/H_2O Analyzer and
215 a LI-7700 open path CH_4 analyzer, both sensors from LI-COR (LI-COR Environmental, Lincoln,
216 NE, USA). All data were collected at 10 Hz, processed in EddyPro 6.2.0 Software from LI-COR
217 (LI-COR Environmental, Lincoln, NE, USA) and corrected for potential misalignments of the
218 anemometer, turbulence fluctuations, and air density fluctuations following AmeriFlux protocols.
219 For this study we used nighttime net ecosystem exchange (NEE) as a representation of
220 ecosystem respiration (Barba et al., 2018; Mahecha et al., 2010) and compared it solely to
221 nighttime soil and creek CO_2 efflux. All available data, both nighttime and daytime, were used
222 for comparing ecosystem-scale CH_4 fluxes to creek CH4 fluxes.

223 Soil CO_2 fluxes (representing total soil respiration) were measured from bare sediments
224 within a vegetated plot every 5 minutes with the eosFD Soil CO_2 Flux Sensor (Eosense,
225 Dartmouth, NS, Canada) at two different locations – approximately 13 and 51 m from the creek
226 bank. The chamber footprint measured 10.2 cm in diameter and measurements from both
227 chambers were averaged together for all analyses. The eosFD uses forced diffusion to regulate
228 gas flow through a diffusive membrane rather than a more traditional mechanical pump, as seen
229 in other closed chamber set-ups (Risk et al., 2011). The water quality parameters (measured in 15
230 min intervals) of temperature, salinity, water level, turbidity, and dissolved oxygen were
231 measured with a YSI 6600 sonde (YSI Inc., Yellow Springs, OH, USA) The weather parameters
232 (measured in 15 minute intervals) of barometric pressure, wind speed, total photosynthetically
233 active radiation, and total precipitation, were measured with a CR1000 Meteorological

Monitoring Station (Campbell Scientific, Logan, UT, USA). Both the water quality and weather parameters followed the Centralized Data Management Protocol from the National Estuarine Research Reserve System (NERRS) (NERRS, 2015). All measurements underwent QA/QC (e.g., check for outliers, data inconsistencies) and were averaged into 30 minute and daily averages for further data analysis.

2.6 Data Analysis

All data was processed and analyzed using R 3.4.3 (R Foundation for Statistical Computing, Vienna, Austria). Nonparametric Kruskal-Wallis tests followed by Dunn post-hoc tests were used for all analyses involving manual GHG flux data. Parametric ANOVA tests followed by Tukey HSD post-hoc tests were used for all other analyses.

A canonical correlation analysis (CCA) using the R *CCA* package (González & Déjean, 2012) was performed on daily averages to test the influence of various independent variables on the dependent variables of creek CO_2 and CH_4 efflux. One CCA was performed using all available data and one was carried out for each phenophase, making for a total of 5 separate analyses. A p-value < 0.05 was used to determine if each CCA found a statistically significant relationship between the independent and dependent variables. The CCA method was chosen as the correlation between CO_2 and CH_4 effluxes can be examined, unlike with two separate multiple linear regressions (Thomas, 1984). This was intended to determine how the selected drivers may affect only one or both GHGs considering potential intercorrelations.

The independent variables consisted of temperature, salinity, water level, turbidity, dissolved oxygen, barometric pressure, wind speed, total photosynthetically active radiation, and total precipitation. The CCA reduced all the independent variables to one independent canonical

variate, and all the dependent variables to one dependent canonical variate (Thomas, 1984). The relationship between all the independent and dependent variables was represented by a linear correlation coefficient calculated between the independent canonical variate and the dependent canonical variate. The contribution of each variable to that overall correlation was represented by the linear correlation coefficient calculated between that variable and its' respective variate.

3 Results

Daily averages of ancillary measurements from March to December were typical of a Mid-Atlantic tidal salt marsh (Figure 1). The greenness index (GI, unitless; 0.34 ± 0.02) peaked on DOY 219 (0.40; 08/07/17) with an initial *Dormant* phase of 116 days, a *Greenup* phenophase of 74 days, a short *Maturity* phenophase of 32 days, a *Senescence* phenophase of 78 days, and a second *Dormant* phenophase of 65 days (Figure 1a). Water temperature (Figure 1b; 17.6 ± 6.87 °C) and GI roughly followed the same seasonal pattern while dissolved oxygen (Figure 1c; 4.62 ± 1.71 mg/l) showed an inverse pattern of being lowest in July (0.36 mg/l) when temperature (29.52 °C) and GI (0.40) were highest. Other measured variables did not show a seasonal pattern, despite having differences among phenophases. Water level (Figure 1e; 0.28 m ± 0.12 above sea level), wind speed (Figure 1d; 1.9 ± 0.89 m/s), and salinity (Figure 1f; 10.0 ± 3.54 ppt) were dominated by shorter period variability (days to weeks) pattern. Salinity did tend to increase slowly during the first half of the record, but no clear seasonal cycle was discernible.

277

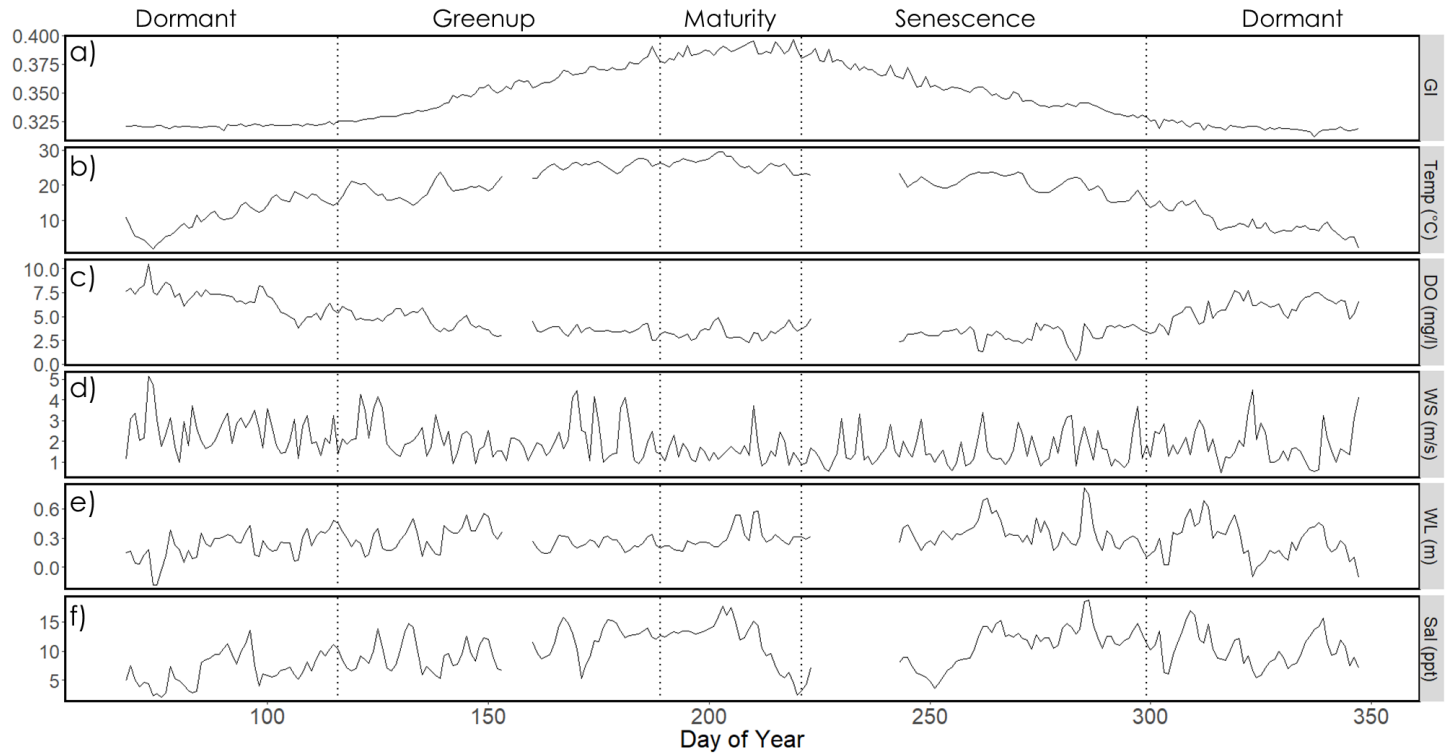

278

279 **Figure 1.** Time series of daily averages of greenness index (a), water temperature (b), dissolved
280 oxygen (c), wind speed (d), water level above sea level (e), and salinity (f) during 2017. The time
281 series are divided into Dormant, Greenup, Maturity, and Senescence phenophases marked by
282 vertical dotted lines.

283

284

285 Modelled creek GHG efflux was tested against the corresponding manual measurements.
286 There were no statistically significant differences between means of modelled (CO_2; 3.88 ± 2.52
287 µmol/m^2/s , CH_4; 25.4 ± 21.6 nmol/m^2/s) and manual measurements (CO_2; 4.11 ± 4.51
288 µmol/m^2/s, CH_4; 28.71 ± 31.93 nmol/m^2/s) overall (i.e., all available measurements) and when
289 analyzed for each tide stage (Kruskal-Wallis test; $p > 0.05$; Figure 2), but manual measurements

had a larger range (CO_2; 0.26 - 20.1 µmol/m^2/s , CH_4; 1.3-123 nmol/m2/s) than modelled values (CO_2; 0.53-8.0 µmol/m^2/s , CH_4; 2.05-66.9 nmol/m^2/s). The magnitude of both manual and modelled GHG fluxes decreased in the order low tide > ebb tide > flood tide > high tide (Kruskal-Wallis test; $p < 0.05$; Figure 2). Gas transfer velocities, standardized to k_{600} values, followed the same tidal pattern and were generally two orders of magnitude smaller for CH_4 (Table 1).

Figure 2. Boxplots comparing modeled and measured efflux of CO_2 (a) and CH_4 (b) divided by tide stage. All box plots by tide stage were significantly different from each other ($p < 0.05$) while there were no statistically significant differences between modelled and measured efflux within each tidal stage ($p > 0.05$).

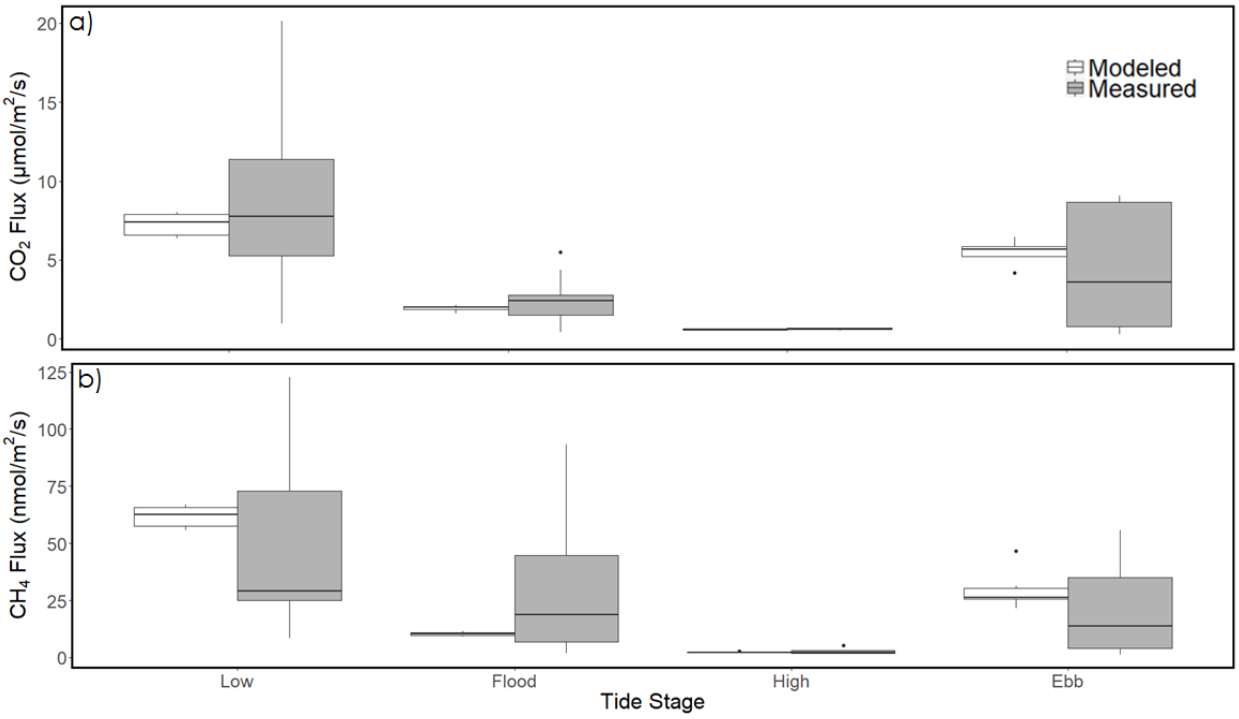

Table 1. Gas Transfer Velocities (k_{600}) of CO_2 and CH_4 by Tide Stage

GHG	High Tide k_{600} (m/d)	Low Tide k_{600} (m/d)	Ebb Tide k_{600} (m/d)	Flood Tide k_{600} (m/d)
CO_2	113.2 +/- 17.8	1330.7 +/- 626.5	1223.9 +/- 328.65	363.2 +/- 98.1
CH_4	2.48 +/- 0.59	61.59 +/- 14.2	29.2 +/- 9.95	10.32 +/- 4.52

303

304 Daily averages of pCO_2 in the creek (8729 ± 622.2 µmol/mol) exhibited a seasonal trend
305 with a peak in the *Maturity* phenophase (Figure 3a). Half-hourly averages of creek pCO_2 were
306 highest at low tide (9110 ± 810 µmol/mol), lowest at high tide (8410 ± 776 µmol/mol), and
307 roughly equal between flood (8730 ± 805) and ebb tides (8690 ± 780 µmol/mol) (Figure 4a-d).
308 Daily averages of modelled creek CO_2 efflux (3.7 ± 0.63 µmol/m^2/s), however, did not show a
309 clear seasonal trend (Fig 3b). Half-hourly averages of modelled creek CO_2 efflux consistently
310 showed higher variability at low tide (7.32 ± 0.52 µmol/m^2/s) than at high tide (0.56 ± 0.04
311 µmol/m^2/s) (Figure 4e-h).

312

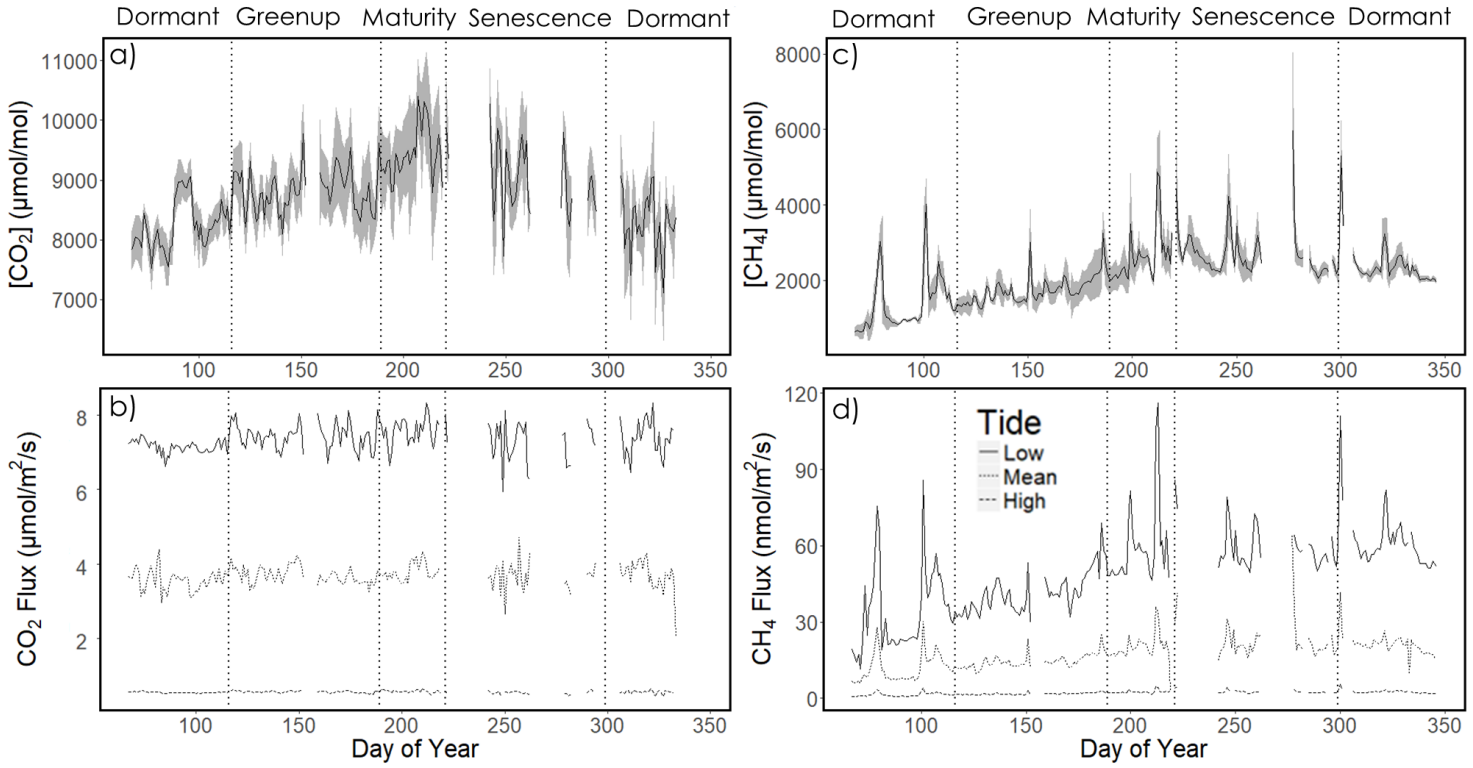

Figure 3. Time series of daily averages of creek pCO_2 (a) and pCH_4 (c). Time series of modelled CO_2 efflux (b) and modelled CH_4 efflux (d) divided into daily averages for high and low tide values, and a daily mean calculated with all available data. The shaded grey area (in a and c) represents the 95% confidence intervals for the daily average. The time series are divided by phenophase into *Dormant*, *Greenup*, *Maturity*, and *Senescence* phenophases marked by vertical dotted lines.

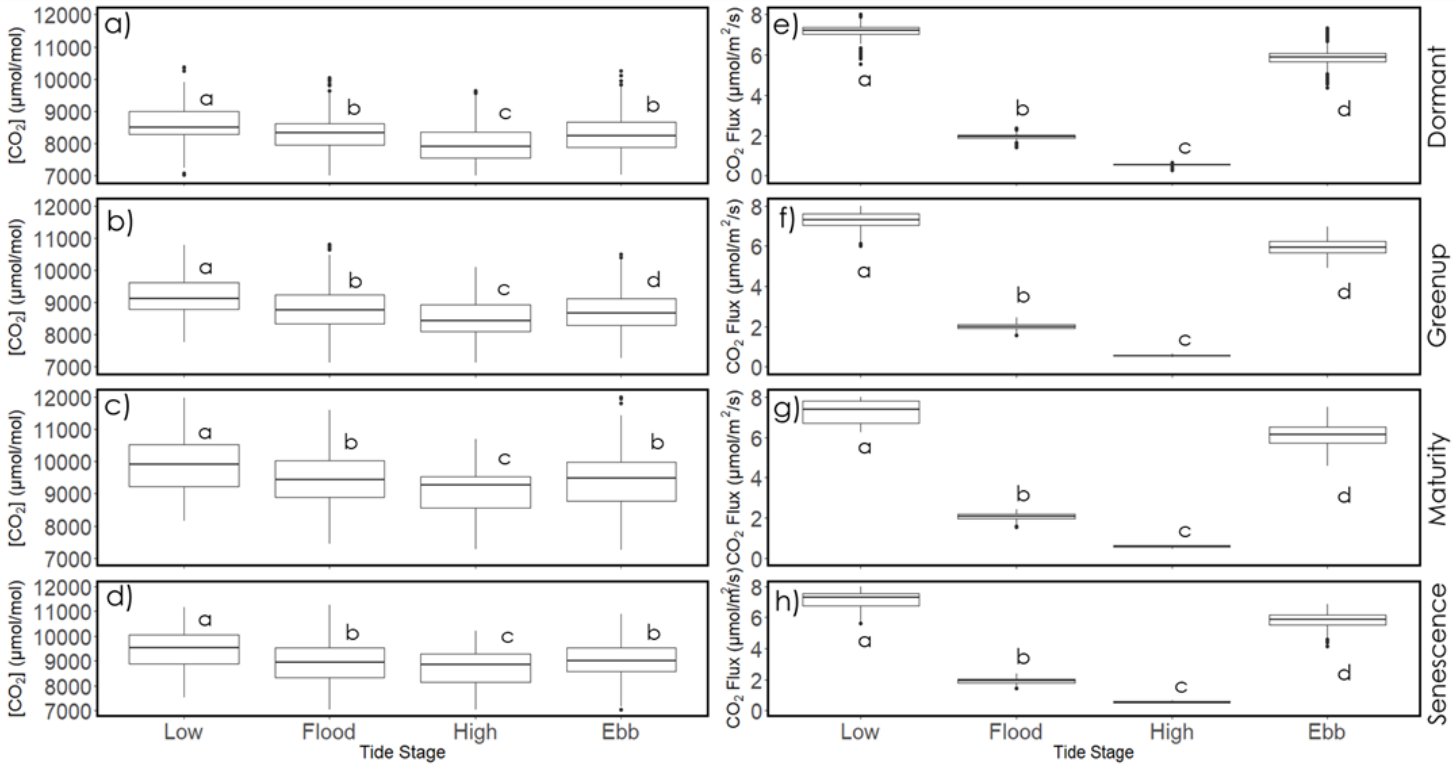

Figure 4. Box plots comparing CO_2 concentration (a-d) or CO_2 flux (e-h) between tide stages for each phenophase: *Dormant* (a, e), *Greenup* (b, f), *Maturity* (c, g), and *Senescence* (d, h). Different letters located above or below each box plot represent statistical significance ($p < 0.05$) among values in that panel.

Daily averages of pCH_4 in the creek (2100 ± 782.9 µmol/mol) exhibited a seasonal trend with a peak in the *Maturity* phenophase and then declined at a slower rate than it peaked (Figure 3c). Half-hourly averages of pCH_4 also demonstrated a slight trend of being highest at high tide (2180 ± 840 µmol/mol), lowest at low tide (1900 ± 7.4 µmol/mol), and roughly equal between

337 flood (2130 ± 898 µmol/mol) and ebb tides (2020 ± 708 µmol/mol) with slight differences in
338 trends between phenophases (Figure 5a-d). Daily averages of modelled CH_4 efflux (17.4 ± 6.9
339 nmol/m^2/s) held a similar seasonal pattern to pCH4 albeit with a lower peak (Figure 3d). Half-
340 hourly averages of modelled creek CH_4 emissions were consistently more variable at low tide
341 (48.5 ± 17.1 nmol/m^2/s) than high tide (2.13 ± 0.78 nmol/m^2/s) (Figure 5e-h).

342

343

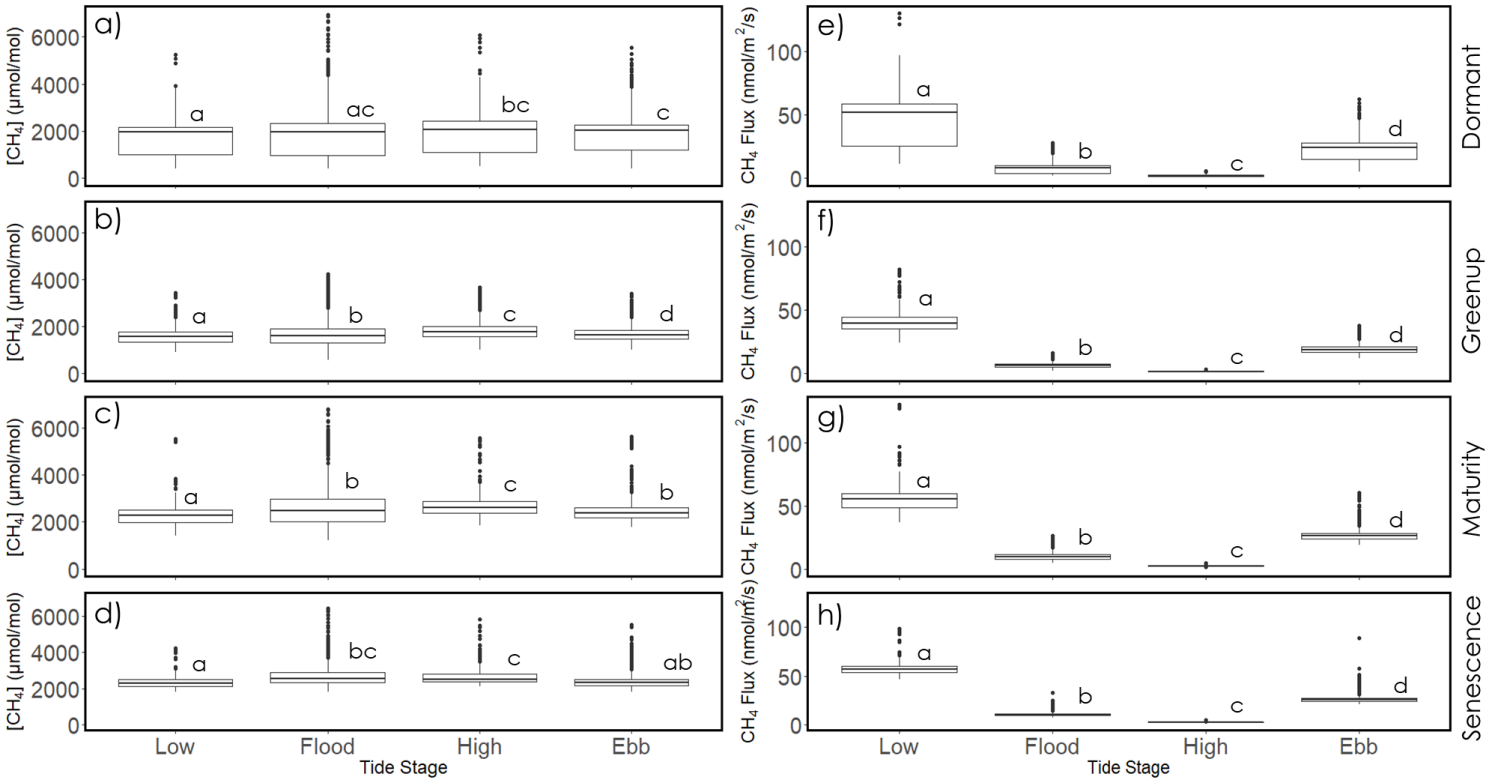

344

345 **Figure 5.** Box plots comparing pCH_4 (a-d) or CH_4 efflux (e-h) between tide stages for each
346 phenophase: Dormant (a, e), Greenup (b, f), Maturity (c, g), and Senescence (d, h). Different
347 letters above each box plot represent statistical significance ($p < 0.05$) among values in that
348 panel.

Statistically significant relationships (CCA; $p < 0.05$) were found between the daily averages of independent variables and modelled GHG efflux during the whole growing season and within each phenophase save for *Senescence* (due to data gaps). During the whole growing season, the CCA showed that dissolved oxygen and wind speed held notable, hereby defined as a statistically significant correlation coefficient > |0.4|, negative correlations with creek CH_4 efflux (Figure 6a). Across phenophases, dissolved oxygen remained a notable factor for creek CH_4 efflux except during the *Maturity* phenophase (Figure 6b-d), and wind speed remained a notable factor for CH_4 efflux only during the *Dormant* phenophase (Figure 6b). Salinity emerged as a notable factor for CH_4 efflux during the *Dormant* and *Greenup* phenophases, solar radiation only during the *Dormant* phenophase, and temperature only during the *Greenup* phenophase (Figure 6b-c). During the *Dormant* phenophase, dissolved oxygen, wind speed, solar radiation, and salinity were also notable factors for CO_2 efflux (Figure 6b). During the Maturity phenophase, turbidity was the only variable notably associated with either GHG (Figure 6d). No notable correlations between any independent variables and creek CO_2 efflux for the whole growing season were found as CO_2 efflux's linear correlation coefficient with the dependent variate was only 0.22 (Figure 6a).

372

373

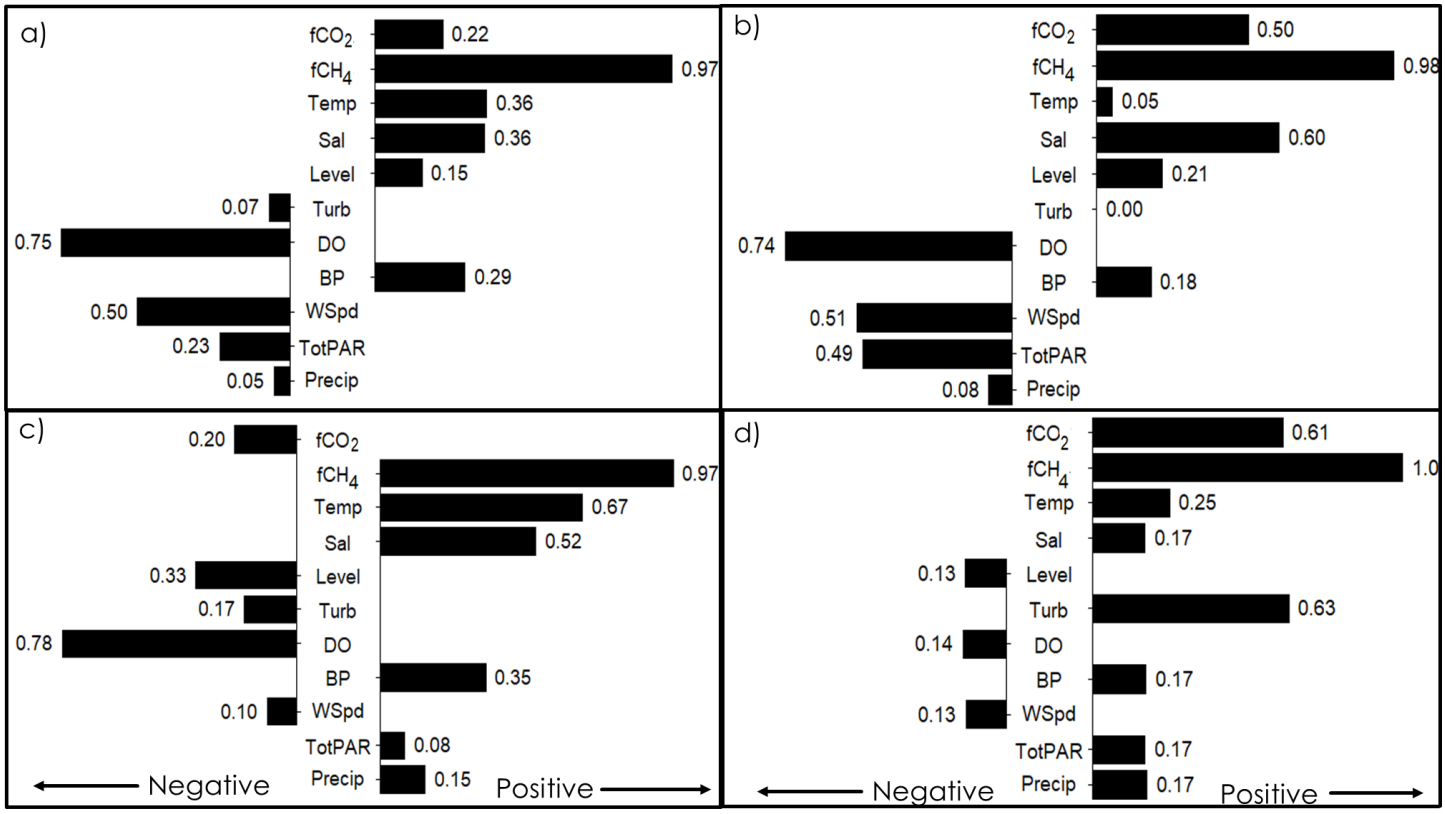

374

375 **Figure 6.** Results of a canonical correlation analysis (CCA) between measured environmental
376 variables and modelled creek CO_2 and CH_4 efflux during: the whole growing season (a),
377 *Dormant* phenophase (b), *Greenup* phenophase (c), the *Maturity* phenophase (d). The
378 *Senescence* phenophase was found to not have any statistically significant relationships between
379 factors ($p > 0.05$). Numbers represent the linear correlation coefficients between factors with
380 negative correlation coefficients going to the left and positive correlation coefficients going to
381 the right. fCO_2 is CO_2 efflux ($\mu mol/m^2/s$), fCH_4 is CH_4 efflux ($nmol/m^2/s$), Temp is water
382 temperature (°C), Sal is salinity (ppt), Level is water level (m), Turb is turbidity (NTU), DO is

383 dissolved oxygen (mg/l), BP is barometric pressure (mb), WSpd is wind speed (m/s), TotPAR is
384 total photosynthetically active radiation (mmol/m^2), and Precip is precipitation (mm).
385
386 Statistically significant differences were found between ecosystem-scale, creek, and
387 sediment efflux within each phenophase for CO_2 and between ecosystem and creek efflux within
388 each phenophase for CH_4 (Figure 7, ANOVA; $p<0.05$). Only CO_2 efflux measurements (for
389 sediment and creek) taken at night-time were considered for comparison with nighttime
390 ecosystem-scale CO_2 efflux measurements (NEE). During the whole year, night-time creek CO_2
391 efflux (3.6 ± 0.63 µmol/m^2/s) was significantly higher than nighttime sediment efflux (1.5 ± 1.23
392 µmol/m^2/s) but lower than nighttime NEE (5.4 ± 3.9 µmol/m^2/s). However, during the *Dormant*
393 period, night-time creek CO_2 efflux (3.7 ± 0.45 µmol/m^2/s) was higher than both night-time
394 sediment efflux (0.95 ± 0.81 µmol/m^2/s) and NEE (2.1 ± 1.1 µmol/m^2/s). Creek CH_4 efflux (17.5
395 ± 6.9 nmol/m^2/s) was consistently lower than ecosystem-scale CH_4 efflux (68.1 ± 52.3
396 nmol/m^2/s) across the whole growing season, with the gap between the two widening as the
397 season progressed.
398

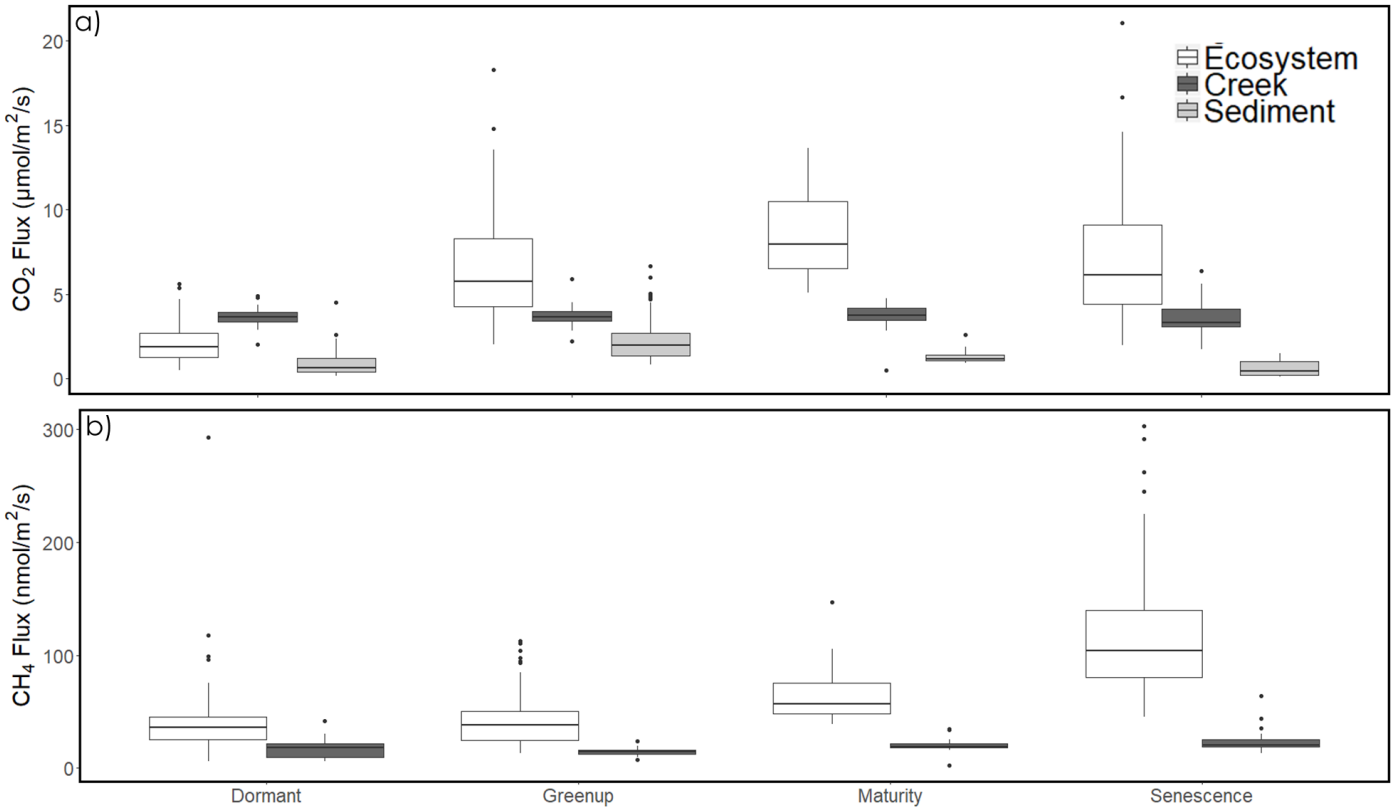

Figure 7. Box plots comparing ecosystem-scale CO_2 efflux (nighttime NEE), creek nighttime CO_2 efflux, and nighttime sediment CO_2 efflux (a). Box plots comparing ecosystem-scale and creek CH_4 fluxes (b). Box plots are arranged based on each phenophase. All box plots within each phenophase were significantly different from each other ($p < 0.05$). Sediment CH_4 efflux was not measured.

4 Discussion

The first hypothesis, that GHG efflux from the creek would peak in the summer, was supported for CH_4 but not for CO_2 as the creek lacked significant seasonal variability for CO_2 efflux but showed some seasonal variability for CH_4 efflux (Figure 3). This differs from observations in temperate terrestrial environments such as forests where both CO_2 and CH_4

411 emissions exhibited strong seasonal trends driven by changing temperatures (Yvon-Durocher et
412 al., 2012, 2014). Inland temperate aquatic environments like rivers have also exhibited seasonal
413 trends in CO_2 efflux (Laruelle et al., 2015). However, the concentrations of both GHGs in the
414 creek did exhibit more of a seasonal pattern than the efflux (Figure 3). The lack of a seasonal
415 trend for GHG efflux compared to the concentrations suggests the influence of confounding and
416 competing factors beyond the concentration gradient between water and air. These factors were
417 tidally linked, likely influencing the gas transfer velocity (*k*; see below), as the efflux of both
418 GHGs differed markedly by tidal stage (Figures 4-5). Both GHG effluxes also lacked the
419 expected high correlations with water temperature (Figure 6), suggesting that creek GHG efflux
420 has drivers that are fundamentally different from those of inland terrestrial and aquatic
421 ecosystems. This lack of temperature dependency should be tested across other salt marsh creeks
422 but, if it proves to be persistent, then this could be an important mathematical and conceptual
423 formulation for ecosystem-process models across terrestrial-aquatic interfaces.

424 The influence of tides may explain why the second hypothesis (that ebb and flood tides
425 would have the highest GHG efflux) was only partially supported. One relevant tidal factor is
426 likely water velocity changing with tide stage. Water velocity has been observed to increase the
427 gas transfer velocity (*k*) of air-water gas efflux in terrestrial streams (Raymond et al., 2012). A
428 higher *k* during flood and ebb tides may explain why there is a higher GHG efflux during those
429 tide stages. Many tidal channels also experience tidal asymmetry between ebb and flood tides
430 (Pethick, 1980) where one stage has a faster velocity than the other. This tidal asymmetry in
431 velocity may explain the observed difference in flux magnitude between ebb and flood tides
432 (Figures 2-4). However, low tide exhibited higher mean efflux than both ebb and flood tide
433 despite its slower velocity. Thus, turbulence may be an additional tidal factor that affects GHG

efflux in tidal creeks. As water level falls in a tidal channel, more flow is directed along the channel axis, rather than across, which generates higher turbulence between the creek bed and the water body (Ralston & Stacey, 2006). Laboratory experiments have demonstrated that increased turbulence at the bottom of water bodies 48-48.6 cm in depth increases the *k* at the surface (Herlina & Jirka, 2008). At low tide, the creek surface can range from 10-28 cm above the creek bed and thus the surface *k* may be more sensitive to turbulence changes at the creek bed. This suggests velocity-based GHG efflux models, as typical for inland streams, will not be accurate for tidal creeks without taking turbulence into account.

Standardized k_{600} values for CO_2 for all tide stages were one to two orders of magnitude higher than those observed in estuaries and deep (>1 m depth) rivers (Bianchi 2006, Borges et al., 2004). High tide k_{600} values were similar to k_{600} values in shallow streams and rivers, flood tide values were three times higher, while low and ebb tide values were an order of magnitude higher than the highest k_{600} values in these shallow systems (Lorke et al., 2015; Raymond et al., 2012). CH_4 k_{600} values fell within the typical range for shallow streams and rivers save for low tide which averaged twice as high as the highest shallow system observations (Lorke et al., 2015). It is likely that tidal creeks have uniquely high k_{600} values due to their shallow depths and the dynamic shifting of velocity and turbulence (Herlina & Jirka, 2008; Ralston & Stacey, 2006; Raymond et al., 2012) due to tides.

The canonical correlation analysis (CCA) allowed us to explore the third hypothesis, that dissolved oxygen and salinity would inhibit CH_4 efflux, at the annual scale and by phenophase. Dissolved oxygen had a negative effect on CH_4 efflux at the annual scale, but also during the *Dormant* and *Greenup* phenophases (Figure 6). These relationships were expected due to the inhibiting effect of oxygen on methanogenesis (Poffenbarger et al., 2011; Tobias & Neubauer,

2009). At the annual scale, wind speed was also an important factor as higher wind speeds can produce more turbulence, aerate the water surface and thus bring more dissolved oxygen into streams (Chu & Jirka, 2003; Gualtieri, et al., 2002). Salinity showed a positive relationship with CH_4 efflux during the *Dormant* and *Greenup* phenophases and no notable relationships at the annual scale or for any other phenophase. This contrasts with the expected negative relationship that has been observed in salinity gradient studies and between salt marshes with differing salinity ranges (Bartlett et al., 2016; Poffenbarger et al., 2011). This apparent contradiction could be explained by the temporal variability of salinity within the creek being smaller in magnitude compared to the spatial variability within and between salt marshes. Despite previous studies having found a strong relationship between temperature and soil CH_4 efflux (Westermann 1993; Yvon-Durocher et al., 2014), our results only supported these observations during the *Greenup* phenophase. This may be due to tides having a strong influence on *k*, which in turn is a stronger control on creek CH_4 efflux than temperature influence.

CO_2 efflux also lacked its expected temperature relationship, likely for the same reason as CH_4 efflux, as the CCA showed no notable correlations for CO_2 efflux at the annual scale (Figure 6). However, during the *Dormant* phenophase, dissolved oxygen, wind speed, solar radiation, and salinity were notable drivers for CO_2 efflux. Both GHG effluxes also had high correlations with each other and the aforementioned drivers during the *Dormant* phenophase (Figure 6). Thus, the relevant drivers for CO_2 efflux may have emerged due to this positive relationship with CH_4 efflux. Both GHG effluxes also held positive relationships with each other and turbidity during the *Maturity* phenophase. The turbidity relationship may represent a pulse of sediments and GHGs entering the creek from the banks with the two events of water level rise seen during the *Maturity* phenophase (Figure 1). These results bring attention to the potential

challenges of modeling GHG fluxes from tidal creeks since there appear to be confounding and competing factors for CH_4 efflux and no clear dominant factors for CO_2 efflux. Identifying consistent key drivers for soil CO_2 and CH_4 efflux under non-stationary conditions (e.g., during wetting-drying and freezing-thawing cycles) has also be proven to be challenging (Kim et al, 2012). Thus, there is a need to provide more information regarding GHGs pulses and trends across terrestrial and aquatic environments.

Nighttime creek CO_2 efflux was higher than nighttime sediment CO_2 efflux and made up a significant portion of ecosystem-scale CO_2 efflux (i.e., nighttime NEE), thus supporting the fourth hypothesis that the creek was a hotspot for CO_2 efflux. Our results support previous observations on point measurements of GHG efflux across different flowing waters of coastal wetlands but expand upon these observations by comparing automated measurements across water, sediments and the ecosystem-scale. For example, a river flowing through a salt marsh was found to have higher CO_2 emissions but slightly lower CH_4 emissions than the bare soil or marsh plants (Yang et al., 2017), which matches our comparatively low creek CH_4 efflux. However, it should be noted that our model does not incorporate ebullition of CH_4, as ebullition is a rapid episodic process (Joyce & Jewell, 2003) that was not captured during our manual measurements. Based on CH_4 ebullition studies of wetland sediments and streams, the model may be underestimating creek CH_4 efflux (Chanton et al., 1989; Crawford et al., 2004). The tidal creeks of mangroves have also shown high pCO_2 and pCH_4 (Call et al., 2015; Linto et al., 2014), but gas transfer velocities *(k)* need to be developed to quantify the effective water-to-atmosphere efflux from these surfaces. Furthermore, this study builds on the evidence that inland streams and rivers have large CO_2 emissions globally (1.8 pG CO_2/yr) relative to their surrounding ecosystems (Lauerwald et al., 2015; Raymond et al., 2013) by suggesting that tidal creeks are

503 also emission hotspots within their respective ecosystems. Therefore, it is critical to constrain the
504 magnitude of water-to-atmosphere fluxes to reduce the large uncertainties in the carbon cycle
505 associated to tidal wetlands (Hayes et al., 2018).

506 We postulate that higher CO_2 efflux at the creek may be due to lateral transport of CO_2
507 from the creek bank (i.e., sediments that get exposed during low tide) into the creek water (as a
508 physical process driven by the tidal patterns) that increases the water-atmosphere CO_2 gradient
509 (Koné & Borges, 2008). Of note is that creek CO_2 efflux during the *Dormant* period was
510 disproportionately high, having a higher mean than ecosystem-scale CO_2 efflux. It is likely that
511 lateral transport of CO_2 from sediments to the creek waters (promoted by tidal patterns) is
512 persistent throughout the year and maintains high CO_2 concentrations and emissions from the
513 tidal creek. The overall ecosystem CO_2 efflux (i.e., nighttime NEE) decreased during the
514 *Dormant* period likely due to low *S. alterniflora* root respiration (Teal & Kanwisher, 1966) from
515 plant senescence, and low microbial heterotrophic respiration from lower temperatures (Yvon-
516 Durocher et al., 2012; Zhang et al., 2013). Therefore, we propose that the influence of physical
517 processes driven by tidal patterns should be included in process-based models for tidal salt
518 marshes and should be taken into consideration when partitioning eddy covariance NEE into
519 gross primary production and ecosystem respiration.

520 Tides can also promote the lateral transport of CH_4 stored in sediments to the creek. It has
521 been reported that sediments at our study site can have CH_4 concentrations >50,000 µmol/mol
522 (Bothfield, 2016), so they can also be a source of CH_4 to the tidal creek. It was not uncommon to
523 measure CH_4 concentrations at 2000 µmol/mol (and up to > 6000 µmol/mol) within the creek, so
524 this opens the following question: where does this CH_4 go? We postulate that tides promote
525 lateral transport of CH_4 stored in sediments of salt marshes to the coastal ocean. This has been

suggested as a mechanism for CH_4 transport in the North Sea of Germany from surrounding tidal flats (Osudar et al., 2015). This hypothesis must be tested across tidal ecosystems around the world.

Finally, the insights gained into the tidal processes affecting creek GHG efflux and its relationship to ecosystem-scale and sediment GHG fluxes would not be possible without high-temporal resolution using automated measurements. Manual measurements can often miss rapid changes in ecological variables like dissolved oxygen (Banas et al., 2005) so automated measurements have been touted to help resolve uncertainties in sediments of salt marshes (Capooci et al., 2019), ecological and carbon cycle models (Hamilton et al., 2014; Vargas et al., 2011). However, manual GHG flux measurements are urgently needed to understand the spatial variability and magnitudes of GHG fluxes across different landscape features of tidal salt marshes around the world. Only a synergistic effort across the scientific community will provide the much-needed information to accurately account for the contribution of wetlands to the global carbon cycle.

5 Conclusions

This study offered unprecedented information of GHG dynamics in a tidal creek using high-temporal resolution automated measurements. Both GHG effluxes from the creek did not exhibit the expected strong temperature-driven seasonal trend, with CO_2 efflux having no trend and CH_4 efflux having a moderate one. We postulate that the physical effects of tidal changes (velocity, turbulence) overshadows the influence of water temperature in determining magnitudes of GHG efflux. Dissolved oxygen exhibited a negative relationship with CH_4 efflux, as expected, while salinity did not due to confounding factors. CO_2 efflux had no consistent

549 drivers across the year, suggesting it will be difficult to model and predict throughout the year.
550 The creek exhibited two times higher CO_2 efflux than the sediments and made up around 66% of
551 the overall CO_2 emissions from the marsh, suggesting creeks are CO_2 emission hotspots within
552 the salt marsh landscape. We postulate that tidal patterns influence the lateral transport of marsh
553 sediment CO_2 and CH_4 into the creek water, and because of the supersaturation of pCO_2 and
554 pCH_4 in the water, there is likely a lateral transport to the coastal ocean. The dynamics of GHG
555 fluxes in tidal marshes are regulated in a fundamentally different way than from terrestrial
556 ecosystems; thus, future ecosystem-process based models should evaluate current assumptions to
557 improve the representation of terrestrial-aquatic interfaces.
558

559 **Acknowledgments and Data**

560 This study was supported by NSF Grant #1652594. We would also like to thank Kari Saint-
561 Laurent and Mike Mensinger for support of our work at the study site; and Daniel Warner, Josep
562 Barba, and Ricardo Llamas help in collecting manual GHG flux measurements. AVL
563 acknowledges support from a CONACyT doctoral fellowships. MC acknowledges support from
564 a DENIN Environmental Fellowship, as well as an NSF Graduate Research Fellowship
565 (#1247394).

566 Plant phenology data can be downloaded from https://phenocam.sr.unh.edu under the site
567 name *stjones*. Eddy covariance CO_2 and CH_4 flux data can be downloaded from
568 https://ameriflux.lbl.gov/ under the site ID US-StJ. Meteorological data can be downloaded from
569 https://cdmo.baruch.sc.edu/ under the site name DELSJMET. Creek pCO_2 and pCH_4, modelled
570 and measured creek CO_2 and CH_4 efflux, soil CO_2 efflux, and water quality data can be
571 downloaded from (to be submitted to Dryad).

References

Banas, D., Grillas, P., Auby, I., Lescuyer, F., Coulet, E., Moreteau, J. C., & Millet, B. (2005). Short time scale changes in underwater irradiance in a wind-exposed lagoon (Vaccarès lagoon, France): Efficiency of infrequent field measurements of water turbidity or weather data to predict irradiance in the water column. *Hydrobiologia*, *551*(1), 3–16. https://doi.org/10.1007/s10750-005-4446-1

Barba, Josep, Alejandro Cueva, Michael Bahn, Greg A. Barron-Gaffordd, Benjamin Bond-Lamberty, Paul J. Hanson, Aline Jaimes, et al. 2018. "Comparing Ecosystem and Soil Respiration: Review and Key Challenges of Tower-Based and Soil Measurements." Agricultural and Forest Meteorology 249 (February): 434–43.

Bartlett, K. B., Bartlett, D. S., Harriss, R. C., Sebacher, D. I., Biogeochemistry, S., & Sebacher, D. I. (2016). Methane Emissions along a Salt Marsh Salinity Gradient. *Biogeochemistry*, *4*(3), 183–202. https://doi.org/10.1007/BF02187365

Baumann, H., Wallace, R. B., Tagliaferri, T., & Gobler, C. J. (2015). Large Natural pH , CO2 and O2 Fluctuations in a Temperate Tidal Salt Marsh on Diel, Seasonal, and Interannual Time Scales. *Estuaries and Coasts*, *38*(1), 220–231. https://doi.org/10.1007/s12237-014-9800-y

Bianchi, T. S. (2006). Dissolved Gases in Water In *Biogeochemistry of Estuaries* (pp. 84-100). Oxford, UK: Oxford University Press.

Bond-lamberty, B., Bailey, V. L., Chen, M., Gough, C. M., & Vargas, R. (2018). Globally rising soil heterotrophic respiration over recent decades. *Nature*, *560*, 80-83.

https://doi.org/10.1038/s41586-018-0358-x

Borges, A.V., Vanderborght, JP., Schiettecatte, LS., Gazeau F., Ferron-Smith, S., Delille, B., & Frankignoulle, M. Variability of the gas transfer velocity of CO2 in a macrotidal estuary (the Scheldt). (2004). *Estuaries*, *27*(4): 593-603. https://doi.org/10.1007/BF02907647

Bothfeld, Frances. (2016). "Spatial and Temporal Heterogeneity of Methane and Carbon Dioxide Production and Flux in a Temperate Tidal Salt Marsh." University of Delaware. https://search.proquest.com/pqdtlocal1006271/docview/1776481154.

Call, M., Maher, D. T., Santos, I. R., Ruiz-Halpern, S., Mangion, P., Sanders, C. J., et al. (2015). Spatial and temporal variability of carbon dioxide and methane fluxes over semi-diurnal and spring-neap-spring timescales in a mangrove creek. *Geochimica et Cosmochimica Acta*, *150*, 211–225. https://doi.org/10.1016/j.gca.2014.11.023

Capooci, M., Barba, J., Seyfferth, A.L., & Vargas, R. (2019). Experimental influence of storm-surge salinity on soil greenhouse gas emissions from a tidal salt marsh. *Science of the Total Environment*, *686*, 1164-1172. https://doi.org/10.1016/j.scitotenv.2019.06.032

Chanton, J. P., Martens, C.S., & Kelley C.A. (1989.) Gas transport from methane-saturated, tidal freshwater and wetland sediments. *Limnology and Oceanography*, *34*(5), 807-819.

Chmura, G. L., Anisfeld, S. C., Cahoon, D. R., & Lynch, J. C. (2003). Global carbon sequestration in tidal, saline wetland soils. *Global Biogeochemical Cycles*, *17*(4), 1111. https://doi.org/10.1029/2002GB001917

Chmura, G. L., Kellman, L., & Guntenspergen, G. R. (2011). The greenhouse gas flux and

potential global warming feedbacks of a northern macrotidal and microtidal salt marsh. *Environmental Research Letters*, *6*(4), 044016. https://doi.org/10.1088/1748-9326/6/4/044016

Chu, C. R., Jirka, G. H., & Asce, F. (2003). Wind and Stream Flow Induced Reaeration. *Journal of Environmental Engineering*, *129*, 1129–1136. 1

Cox, T. & Schepers, L. (2017). Tides: Quasi-Periodic Time Series Characteristics. R package version 2.0. https://CRAN.R-project.org/package=Tides

Crawford, J.T., Stanley E.H., Spawn A.S., Finlay, J.C., Loken L.C., & Striegel, R.G. (2014). Ebullitive methane emissions from oxygenated wetland streams. *Global Change Biology*, *20*, 3408-3422. doi: 10.1111/gcb.12614

Delaware Department of Natural Resources and Environmental Control (1999). *DELAWARE NATIONAL ESTUARINE RESEARCH RESERVE ESTUARINE PROFILE*. Dover, DE: National Oceanic and Atmospheric Administration.

Dausse, A., Garbutt, A., Norman, L., Papadimitriou, S., Jones, L.M., Robins, P.E., & Thomas, D.N. (2012). Biogeochemical functioning of grazed estuarine tidal marshes along a salinity gradient. *Estuarine, Coastal and Shelf Science*, *100*, 83-92. https://doi.org/10.1016/j.ecss.2011.12.037

Fagherazzi, S., Wiberg, P. L., Temmerman, S., Struyf, E., Zhao, Y., & Raymond, P. A. (2013). Fluxes of water, sediments, and biogeochemical compounds in salt marshes. *Ecological Processes*, *2*(1), 3. https://doi.org/10.1186/2192-1709-2-3

633 Filippa, G., Cremonese, E., Migliavacca, M., Galvagno, M., Forkel, M., Wingate, L., …
634 Richardson, A. D. (2016). Phenopix: A R package for image-based vegetation phenology.
635 *Agricultural and Forest Meteorology, 220*, 141–150.
636 https://doi.org/10.1016/j.agrformet.2016.01.006

637 Flanagan L.B. (2009) Phenology of Plant Production in the Northwestern Great Plains:
638 Relationships with Carbon Isotope Discrimination, Net Ecosystem Productivity and
639 Ecosystem Respiration. In: Noormets A. (eds) *Phenology of Ecosystem Processes*. Springer,
640 New York, NY

641 Forbrich, I., & Giblin, A. E. (2015). Marsh-atmosphere CO2exchange in a New England salt
642 marsh. *Journal of Geophysical Research G: Biogeosciences*, *120*(9), 1825–1838.
643 https://doi.org/10.1002/2015JG003044

644 Forbrich, I., Giblin, A. E., & Hopkinson, C. S. (2018). Constraining Marsh Carbon Budgets
645 Using Long-Term C Burial and Contemporary Atmospheric CO2 Fluxes. *Journal of*
646 *Geophysical Research: Biogeosciences*, *123*(3), 867–878.
647 https://doi.org/10.1002/2017JG004336

648 Gillespie, A. R., Kahle, A. B., & Walker, R. E. (1987). Color Enhancement of Highly Correlated
649 Images. II. Channel Ratio and "Chromaticity" Transformation Techniques. *Remote Sensing*
650 *of Environment*, *22*(3), 343–365. https://doi.org/10.1016/0034-4257(87)90088-5

651 González, I. & Déjean, S. (2012). CCA: Canonical correlation analysis. R package version
652 1.2.https://CRAN.R-project.org/package=CCA

653 Gualtieri, C., Gualtieri, P., & Doria, G. P. (2002). Dimensional Analysis of Reaeration Rate in

Streams. *Journal of Environmental Engineering*, *128*(1), 12–18.

Greenwood, D.J. (1961). THE EFFECT OF OXYGEN CONCENTRATION ON THE DECOMPOSITION OF ORGANIC MATERIALS IN SOIL. *Plant and Soil*, *14*(4), 360-376.

Hamilton, D. P., Carey, C. C., Arvola, L., Arzberger, P., Cole, J. J., Gaiser, E., … Lin, F. (2015). A Global Lake Ecological Observatory Network (GLEON) for synthesising high-frequency sensor data for validation of deterministic ecological models A Global Lake Ecological Observatory Network (GLEON) for synthesising high-frequency sensor data for validation of deterministic ecological models. *Inland Waters*, 5(1), 49-56. https://doi.org/10.5268/IW-5.1.566

Hayes DJ, Vargas R, Alin SR, Conant RT, Hutyra LR, Jacobson AR, et al. Chapter 2: The North American carbon budget. In: Cavallaro N, Shrestha G, Birdsey R, Mayes MA, Najjar RG, Reed SC, et al., editors. Second State of the Carbon Cycle Report (SOCCR2): A Sustained Assessment Report Washington, DC, USA,: U.S. Global Change Research Program; 2018. p. 71-108, https://doi.org/10.7930/SOCCR2.2018.Ch2.

Herlina, & Jirka, G. H. (2008). Experiments on gas transfer at the air-water interface induced by oscillating grid turbulence. *Journal of Fluid Mechanics*, *594*, 183–208. https://doi.org/10.1017/S0022112007008968

Howard, J., Sutton-Grier, A., Herr, D., Kleypas, J., Landis, E., Mcleod, E., … Simpson, S. (2017). Clarifying the role of coastal and marine systems in climate mitigation. *Frontiers in Ecology and the Environment*, *15*(1), 42–50. https://doi.org/10.1002/fee.1451

675 Huertas, I. E., Flecha, S., Figuerola, J., Costas, E., & Morris, E. P. (2017). Effect of hydroperiod
676 on CO_2 fluxes at the air-water interface in the Mediterranean coastal wetlands of Doñana.
677 *Journal of Geophysical Research: Biogeosciences*, 1615–1631.
678 https://doi.org/10.1002/2017JG003793

679 Jones, S. F., Stagg, C. L., Krauss, K. W., & Hester, M. W. (2018). Flooding Alters Plant-
680 Mediated Carbon Cycling Independently of Elevated Atmospheric CO2Concentrations.
681 *Journal of Geophysical Research: Biogeosciences*, *123*(6), 1976–1987.
682 https://doi.org/10.1029/2017JG004369

683 Joyce, J. & Jewell, P.W. (2003). Physical Controls on Methane Ebullition from Reservoirs and
684 Lakes. *Environmental and Engineering Geoscience, 9*(2), 167-168.

685 Kim, D. G., R. Vargas, B. Bond-Lamberty, and M. R. Turetsky. 2012. "Effects of Soil Rewetting
686 and Thawing on Soil Gas Fluxes: A Review of Current Literature and Suggestions for
687 Future Research." *Biogeosciences* 9 (7): 2459–83.

688 Kirwan, M. L., Guntenspergen, G. R., & Langley, J. A. (2014). Temperature sensitivity of
689 organic-matter decay in tidal marshes. *Biogeosciences*, *11*(17), 4801–4808.
690 https://doi.org/10.5194/bg-11-4801-2014

691 Koné, Y. J. M., & Borges, A. V. (2008). Dissolved inorganic carbon dynamics in the waters
692 surrounding forested mangroves of the Ca Mau Province (Vietnam). *Estuarine, Coastal and*
693 *Shelf Science, 77*(3), 409–421. https://doi.org/10.1016/j.ecss.2007.10.001

694 Lauerwald, R., G. G. Laruelle, J. Hartmann, P. Ciais, and P. A. G. Regnier (2015), Spatial
695 patterns in CO2 evasion from the global river network, *Global Biogeochemical Cycles, 29*,

534–554, doi:10.1002/ 2014GB004941.

Laruelle, G. G., Lauerwald, R., Rotschi, J., Raymond, P. A., Hartmann, J., & Regnier, P. (2015). Seasonal response of air–water CO2 exchange along the land–ocean aquatic continuum of the northeast North American coast. *Biogeosciences*, *12*, 1447–1458. https://doi.org/10.5194/bg-12-1447-2015

Linto, N., Barnes, J., Ramachandran, R., Divia, J., Ramachandran, P., & Upstill-Goddard, R. C. (2014). Carbon Dioxide and Methane Emissions from Mangrove-Associated Waters of the Andaman Islands, Bay of Bengal. *Estuaries and Coasts*, *37*(2), 381–398. https://doi.org/10.1007/s12237-013-9674-4

Lorke, A., Bodmer, P., Noss, C., Alshboul, Z., Koschorrek, M., Somlai-Haase, C., et al. Technical Note: Drifting versus Anchored Flux Chambers for Measuring Greenhouse Gas Emissions from Running Waters. (2015) *Biogeosciences*, *12*(23), 7013–7024. https://doi:10.5194/bg-12-7013-2015.

Macreadie, P. I., Hughes, A. R., & Kimbro, D. L. (2013). Loss of "Blue Carbon" from Coastal Salt Marshes Following Habitat Disturbance. *PLoS ONE*, *8*(7), 1–8. https://doi.org/10.1371/journal.pone.0069244

Mahecha, M. D., Reichstein, M., Carvalhais, N., Lasslop, G., Lange, H., Seneviratne, S. I., …Richardson, A. D. (2010). Global Convergence in the Temperature Sensitivity of Respiration at Ecosystem Level. *Science*, *329*, 838–840.

McLeod, E., Chmura, G. L., Bouillon, S., Salm, R., Björk, M., Duarte, C. M., … Silliman, B. R. (2011). A blueprint for blue carbon: Toward an improved understanding of the role of

717 vegetated coastal habitats in sequestering CO2. *Frontiers in Ecology and the Environment*,
718 *9*(10), 552–560. https://doi.org/10.1890/110004

719 Moffett, K. B., Wolf, A., Berry, J. A., & Gorelick, S. M. (2010). Salt marsh-atmosphere
720 exchange of energy, water vapor, and carbon dioxide: Effects of tidal flooding and
721 biophysical controls. *Water Resources Research*, *46*(10), 1–18.
722 https://doi.org/10.1029/2009WR009041

723 Moseman-Valtierra, S. Reconsidering the climatic role of marshes: Are they sinks or sources of
724 greenhouse gases? (2012). In *Marshes: Ecology, Management and Conservation*. Nova
725 Scientific Publishers; Hauppauge, NY, USA:. 1–48.

726 Neubauer, S. C., & Anderson, I. C. (2003). Transport of dissolved inorganic carbon from a tidal
727 freshwater marsh to the York River estuary. *Limnology and Oceanography*, *48*(1), 299–307.

728 Osudar, R., Matou, A., Alawi, M., Wagner, D., & Bussmann, I. (2015). Environmental factors
729 affecting methane distribution and bacterial methane oxidation in the German Bight (North
730 Sea). *Estuarine , Coastal and Shelf Science*, *160*, 10–21.
731 https://doi.org/10.1016/j.ecss.2015.03.028

732 Pearson, A. J., Pizzuto, J. E., & Vargas, R. (2016). Influence of run of river dams on f oodplain
733 sediments and carbon dynamics. *Geoderma*, *272*, 51–63.
734 https://doi.org/10.1016/j.geoderma.2016.02.029

735 Pendleton, L., Donato, D. C., Murray, B. C., Crooks, S., Jenkins, W. A., Sifleet, S., … Baldera,
736 A. (2012). Estimating Global “Blue Carbon” Emissions from Conversion and Degradation
737 of Vegetated Coastal Ecosystems. *PLoS ONE*, *7*(9).

https://doi.org/10.1371/journal.pone.0043542

Pethick, J. S. (1980). Velocity surges and asymmetry in tidal channels. *Estuarine and Coastal Marine Science*, *11*(3), 331–345. https://doi.org/10.1016/S0302-3524(80)80087-9

Poffenbarger, H. J., Needelman, B. A., & Megonigal, J. P. (2011). Salinity Influence on Methane Emissions from Tidal Marshes. *Wetlands*, *31*(5), 831–842. https://doi.org/10.1007/s13157-011-0197-0

Raich, J.W. & Schlesinger, W.H. (1992). The global carbon dioxide flux in soil respiration and its relationship to vegetation and climate. *Tellus*, *44*, 81-99.

Ralston, D. K., & Stacey, M. T. (2006). Shear and turbulence production across subtidal channels. *Journal of Marine Research*, *64*(1), 147–171.

Rawitch, M. J. (2015). STREAM CO2 DEGASSING: REVIEW OF METHODS AND LABORATORY VALIDATION OF FLOATING CHAMBERS (Unpublished doctoral dissertation). University of Kansas, Lawrence, Kansas.

Raymond, P. A., Hartmann, J., Lauerwald, R., Sobek, S., McDonald, C., Hoover, M., … Guth, P. (2013). Global carbon dioxide emissions from inland waters. *Nature*, *503*(7476), 355–359. https://doi.org/10.1038/nature12760

Raymond, P. A., Zappa, C. J., Butman, D., Bott, T. L., Potter, J., Mulholland, P., et al. (2012). Scaling the gas transfer velocity and hydraulic geometry in streams and small rivers. *Limnology and Oceanography: Fluids and Environments*, *2*(1), 41–53. https://doi.org/10.1215/21573689-1597669

758 Richardson A. D., Andy B. T., Ciais P., Delbart N., Friedl M. A., Gobron N., et al. (2010)
759 Influence of spring and autumn phenological transitions on forest ecosystem productivity
760 *Philospohical Transactions of the Royal Society B, 365*, 1555.
761 http://doi.org/10.1098/rstb.2010.0102

762 Risk, D., Nickerson, N., Creelman, C., Mcarthur, G., & Owens, J. (2011). Agricultural and
763 Forest Meteorology Forced Diffusion soil flux : A new technique for continuous monitoring
764 of soil gas efflux. *Agricultural and Forest Meteorology*, *151*(12), 1622–1631.
765 https://doi.org/10.1016/j.agrformet.2011.06.020

766 Ruiz-Fernández, A. C., Carnero-Bravo, V., Sanchez-Cabeza, J. A., Pérez-Bernal, L. H., Amaya-
767 Monterrosa, O. A., Bojórquez-Sánchez, S., … Marmolejo-Rodríguez, A. J. (2018). Carbon
768 burial and storage in tropical salt marshes under the influence of sea level rise. *Science of*
769 *The Total Environment*, *630*, 1628–1640. https://doi.org/10.1016/j.scitotenv.2018.02.246

770 Soil Survey Staff NRCS, United States Department of Agriculture. (2019) Web Soil Survey.
771 https://websoilsurvey.sc.egov.usda.gov/App/HomePage.htm

772 Seyednasrollah, B., Young, A.M., Hufkens, K., Milliman, T., Friedl, M.A., Frolking, S., …
773 Zona, D. 2019. PhenoCam Dataset v2.0: Vegetation Phenology from Digital Camera
774 Imagery, 2000-2018. ORNL DAAC, Oak Ridge, Tennessee, USA.
775 https://doi.org/10.3334/ORNLDAAC/1674

776 Teal, J. M., & Kanwisher, J. W. (1966). Gas transport in the marsh grass, Spartina alterniflora.
777 *Journal of Experimental Botany*, *17*(2), 355–361. https://doi.org/10.1093/jxb/17.2.355

778 Thomas, B. (1984) Canonical Correlation Analysis: Uses and Interpretation. Thousand Oaks,

779 California: Sage Publications.

780 Tobias, C., & Neubauer, S. (2009). *Chapter 16 - Salt Marsh Biogeochemistry - An Overview*.
781 *COASTAL WETLANDS: An Integrated Ecosystem Approach* (First edit, Vol. 76). Elsevier.
782 https://doi.org/10.1016/B978-0-444-53103-2.00016-8

783 Tong, C., Huang, J.F., Hu Z.Q., & Jin, Y.F. (2013). Diurnal Variations of Carbon Dioxide,
784 Methane, and Nitrous Oxide Vertical Fluxes in a Subtropical Estuarine Marsh on Neap and
785 Spring Tide Days. Estuaries and Coasts, 36, 633-642. https://doi.org/10.1007/s12237-013-
786 9596-1

787 Tong, C., Wang, W.-Q., Zeng, C.-S., & Marrs, R. (2010). Methane (CH4) emission from a tidal
788 marsh in the Min River estuary, southeast China. *Journal of Environmental Science and*
789 *Health. Part A, Toxic/Hazardous Substances & Environmental Engineering*, *45*(4), 506–16.
790 https://doi.org/10.1080/10934520903542261

791 Van Dam, B. R., Edson, J. B., & Tobias, C. (2019). Parameterizing air-water gas exchange in the
792 shallow, microtidal New River estuary. *Journal of Geophysical Research: Biogeosciences*,
793 *124*, 2351–2363. https://doi.org/ 10.1029/2018JG004908

794 Vargas, R., & Carbone, M. S. (2011). Frontiers and challenges in soil respiration research : from
795 measurements to model-data integration. *Biogeochemistry*, *102*(1-3) 1–13.
796 https://doi.org/10.1007/s10533-010-9462-1

797 Wang, Z. A., & Cai, W. J. (2004). Carbon dioxide degassing and inorganic carbon export from a
798 marsh-dominated estuary (the Duplin River): A marsh CO2 pump. *Limnology and*
799 *Oceanography*, *49*(2), 341–354. https://doi.org/10.4319/lo.2004.49.2.0341

800 Wang, Z. A., Kroeger, K. D., Ganju, N. K., Gonneea, M. E., & Chu, S. N. (2016). Intertidal salt
801 marshes as an important source of inorganic carbon to the coastal ocean. *Limnology and*
802 *Oceanography*, *61*(5), 1916–1931. https://doi.org/10.1002/lno.10347

803 Wanninkhof, R. (2014). Relationship between wind speed and gas exchange over the ocean
804 revisited. *Limnology and Oceanography: Methods*, *12*, 351-362.

805 Warner, D. L., Villarreal, S., Mcwilliams, K., Inamdar, S., & Vargas, R. (2017). Carbon Dioxide
806 and Methane Fluxes From Tree Stems , Coarse Woody Debris , and Soils in an Upland
807 Temperate Forest. *Ecosystems*, *20*(6), 1205–1216. https://doi.org/10.1007/s10021-016-
808 0106-8

809 Westermann, P. (1993). Temperature Regulation of Methane in Wetlands. *Chemosphere*, *26*,
810 321-328.

811 C. Wu, J.M. Chen, T.A. Black, D.T. Price, W.A. Kurz, A.R. Desai, et al. (2013) Interannual
812 variability of net ecosystem productivity in forests is explained by carbon flux phenology in
813 autumn. *Global Ecology & Biogeography*, *22*, 994-1006. https://doi.org/10.1111/geb.12044

814 Yang, W. Bin, Yuan, C. S., Tong, C., Yang, P., Yang, L., & Huang, B. Q. (2017). Diurnal
815 variation of CO2, CH4, and N2O emission fluxes continuously monitored in-situ in three
816 environmental habitats in a subtropical estuarine wetland. *Marine Pollution Bulletin*,
817 *119*(1), 289–298. https://doi.org/10.1016/j.marpolbul.2017.04.005

818 Yvon-Durocher, G., Allen, A. P., Bastviken, D., Conrad, R., Gudasz, C., St-Pierre, A., … del
819 Giorgio, P. A. (2014). Methane fluxes show consistent temperature dependence across
820 microbial to ecosystem scales. *Nature*, *507*(7493), 488–491.

https://doi.org/10.1038/nature13164

Yvon-Durocher, G., Caffrey, J. M., Cescatti, A., Dossena, M., Giorgio, P. Del, Gasol, J. M., … Allen, A. P. (2012). Reconciling the temperature dependence of respiration across timescales and ecosystem types. *Nature*, *487*(7408), 472–476. https://doi.org/10.1038/nature11205

Zhang, Q., Lei, H.M., Yang, D.W. (2013). Seasonal variations in soil respiration, heterotrophic respiration and autotrophic respiration of a wheat and maize rotation cropland in the North China Plain. *Agricultural and Forest Meteorology*, *180*, 34-43. https://doi.org/10.1016/j.agrformet.2013.04.028.

Zhong, Q., Du, Q., Gong, J., Zhang, C., & Wang, K. (2013). Effects of in situ experimental air warming on the soil respiration in a coastal salt marsh reclaimed for agriculture. *Plant and Soil*, *371*(1–2), 487–502. https://doi.org/10.1007/s11104-013-1707-z

Figure 1.

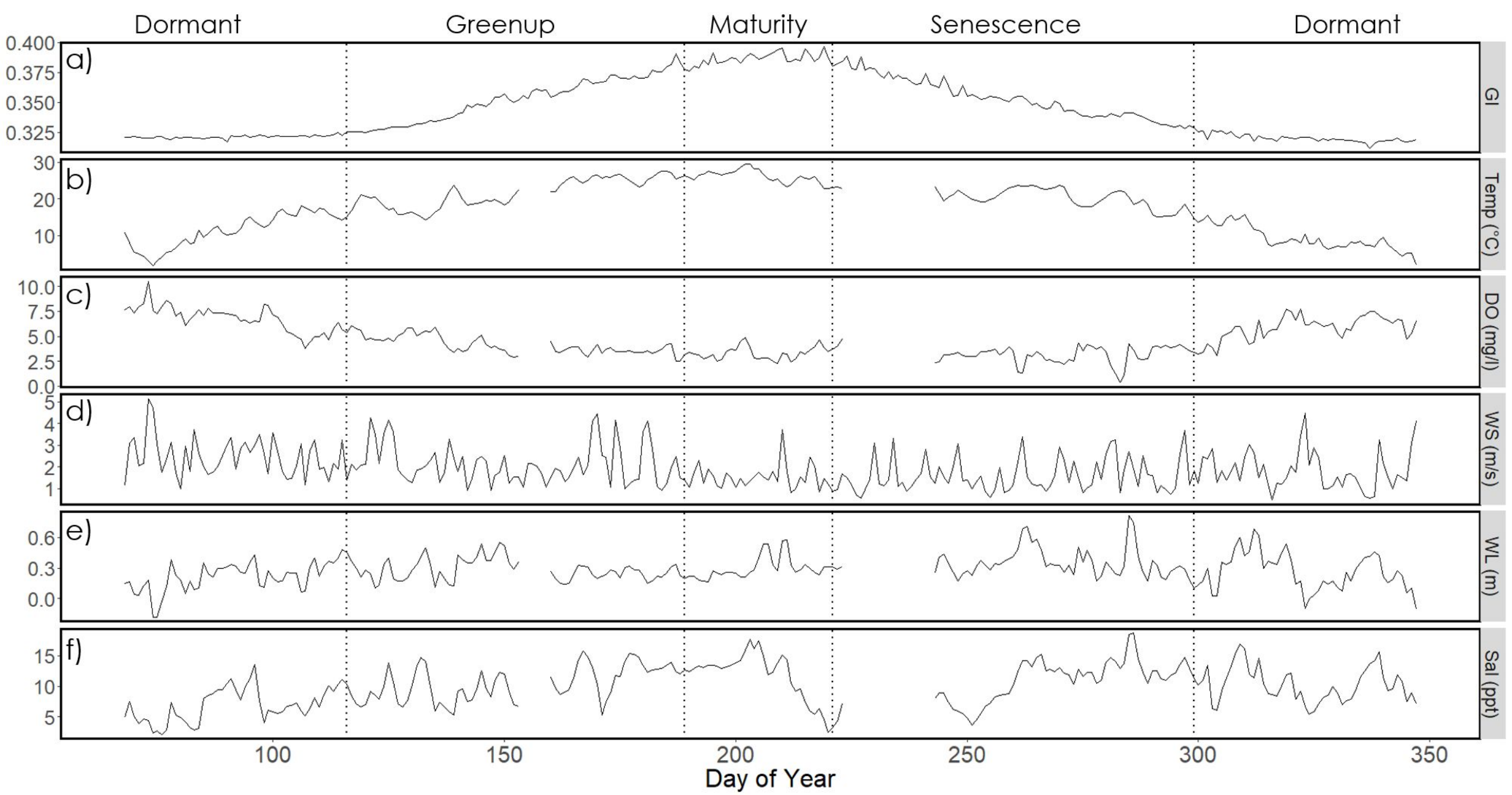
Dormant
Greenup
Maturity
Senescence
Dormant
a)
b)
c)
d)
e)
f)
GI
Temp (°C)
DO (mg/l)
WS (m/s)
WL (m)
Sal (ppt)
0.400
0.375
0.350
0.325
30
20
10
10.0
7.5
5.0
2.5
0.0
5
4
3
2
1
0.6
0.3
0.0
15
10
5
100
150
200
250
300
350
Day of Year

Figure 2.

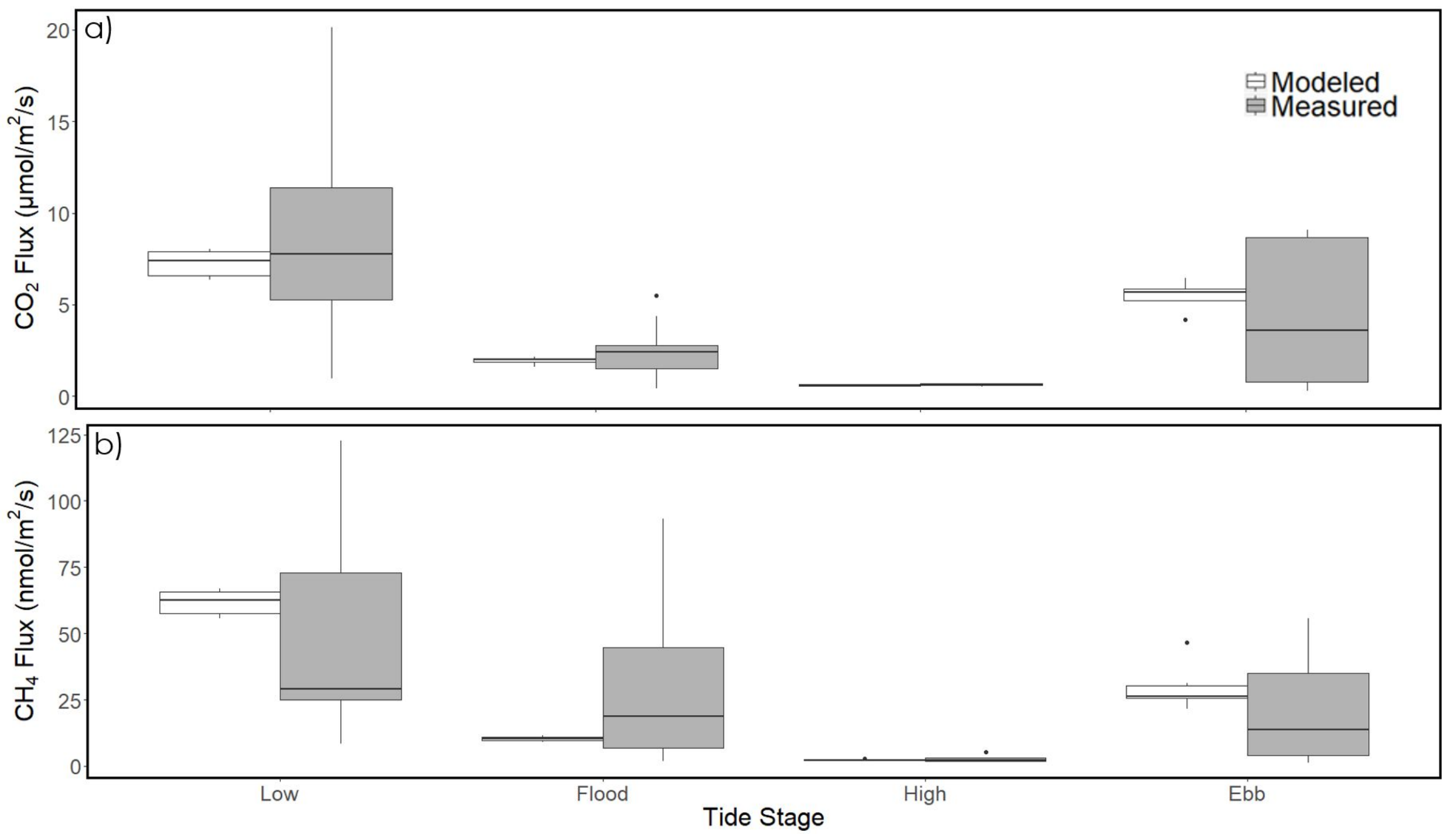
a)
b)
Modeled
Measured
CO_2 Flux (µmol/m^2/s)
CH_4 Flux (nmol/m^2/s)
0
5
10
15
20
25
50
75
100
125
Low
Flood
High
Ebb
Tide Stage

Figure 3.

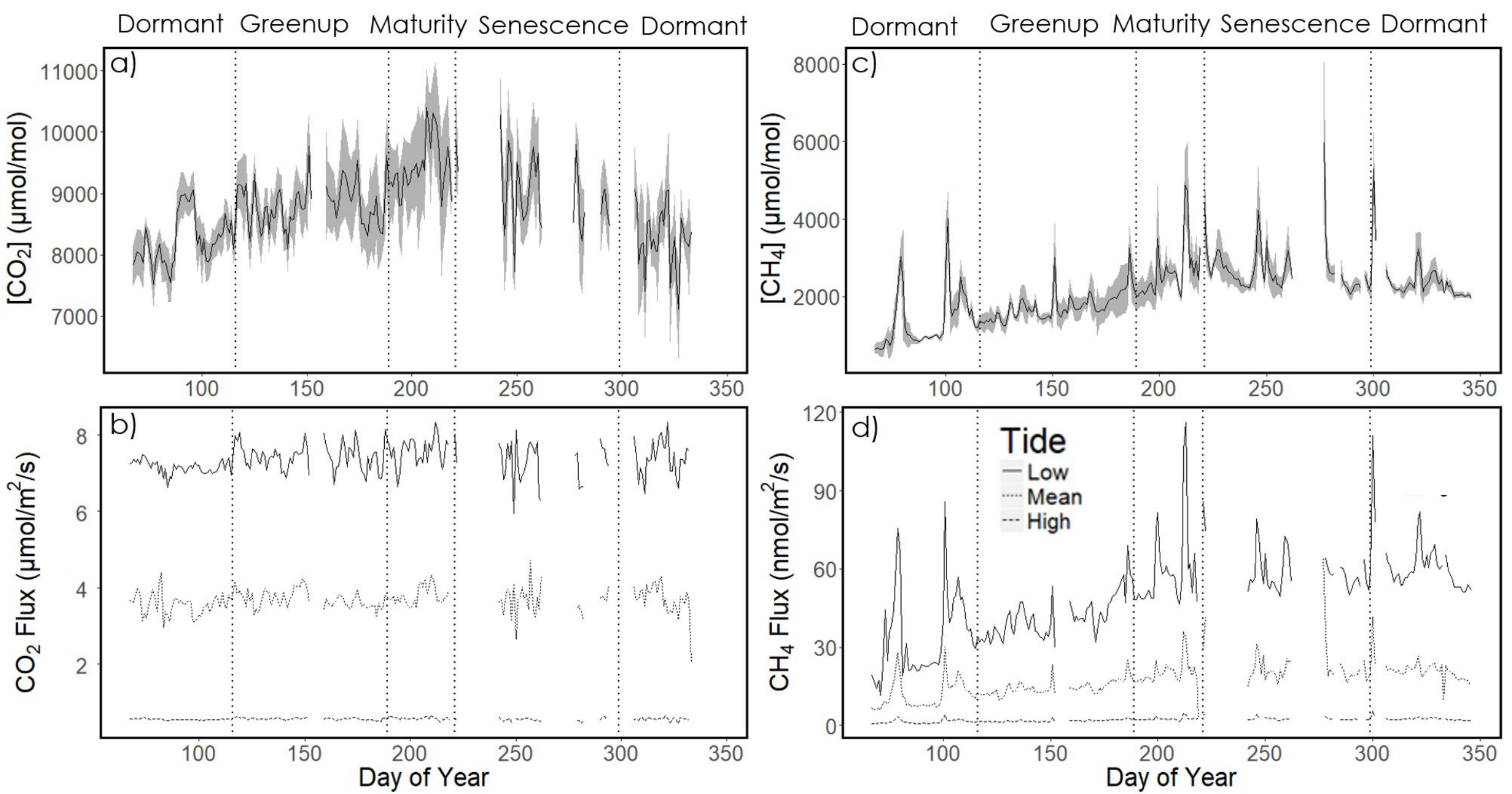
Dormant
Greenup
Maturity
Senescence
Dormant
a)
b)
c)
d)
[CO2] (µmol/mol)
CO2 Flux (µmol/m2/s)
[CH4] (µmol/mol)
CH4 Flux (nmol/m2/s)
Day of Year
Tide
Low
Mean
High

Figure 4.

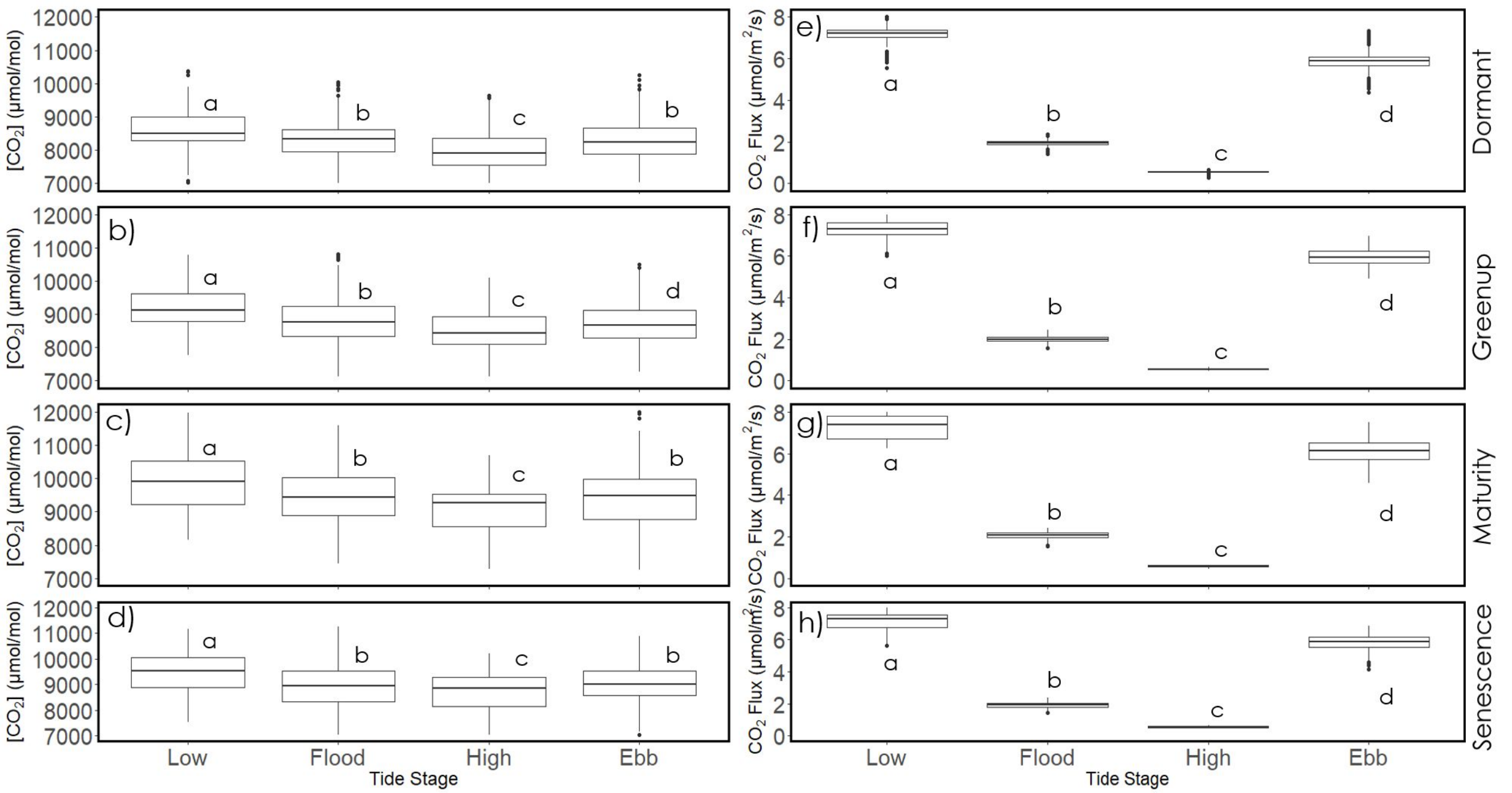
b)
c)
d)
e)
f)
g)
h)
[CO2] (µmol/mol)
CO2 Flux (µmol/m2/s)
12000
11000
10000
9000
8000
7000
8
6
4
2
0
a
b
c
d
Low
Flood
High
Ebb
Tide Stage
Dormant
Greenup
Maturity
Senescence

Figure 5.

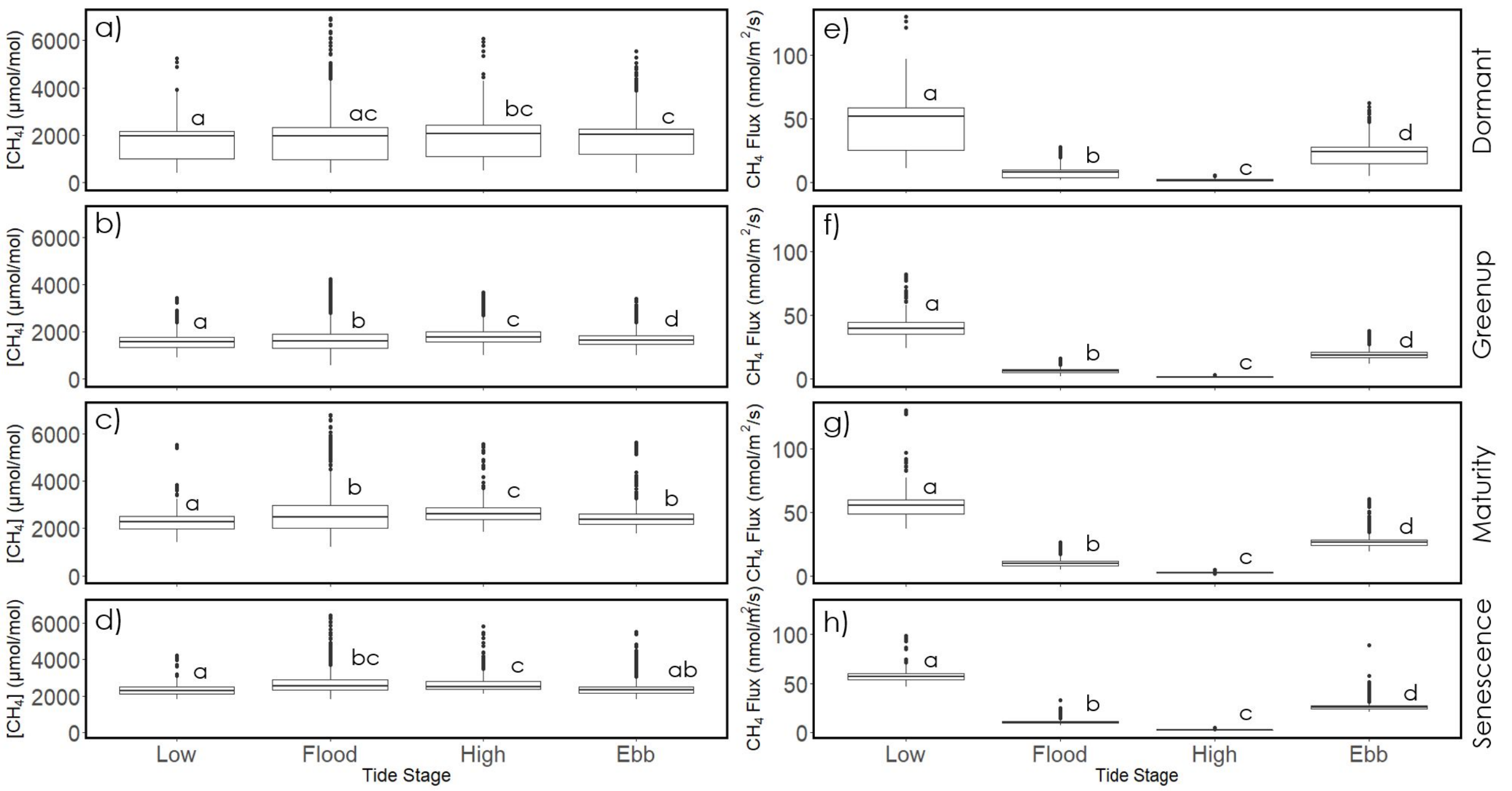
a)
b)
c)
d)
e)
f)
g)
h)
[CH4] (µmol/mol)
CH4 Flux (nmol/m2/s)
0
2000
4000
6000
50
100
a
ac
bc
c
b
d
ab
Low
Flood
High
Ebb
Tide Stage
Dormant
Greenup
Maturity
Senescence

Figure 6.

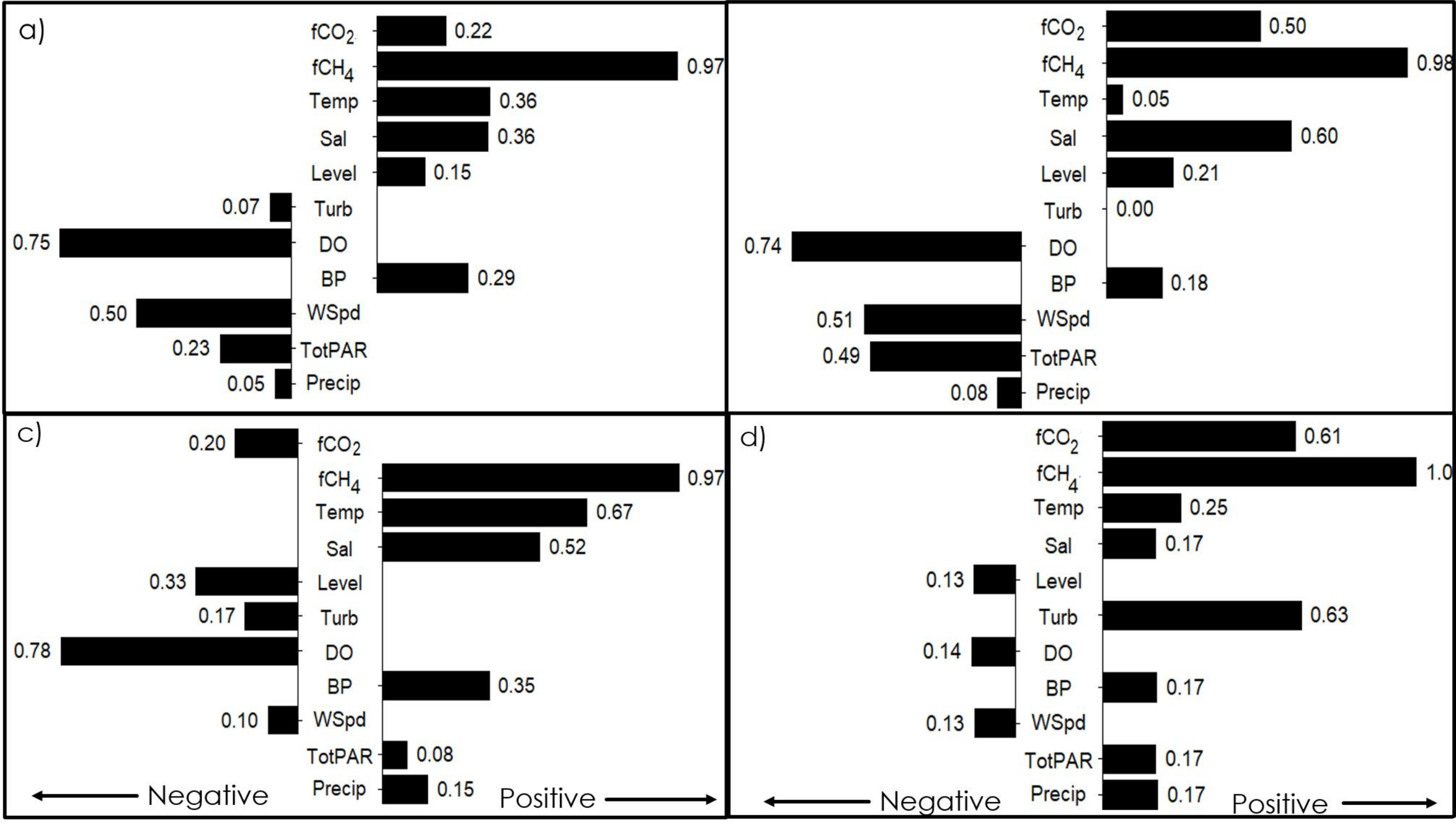
a)
fCO2
fCH4
Temp
Sal
Level
Turb
DO
BP
WSpd
TotPAR
Precip
0.22
0.97
0.36
0.36
0.15
0.07
0.75
0.29
0.50
0.23
0.05
b)
fCO2
fCH4
Temp
Sal
Level
Turb
DO
BP
WSpd
TotPAR
Precip
0.50
0.98
0.05
0.60
0.21
0.00
0.74
0.18
0.51
0.49
0.08
c)
fCO2
fCH4
Temp
Sal
Level
Turb
DO
BP
WSpd
TotPAR
Precip
0.20
0.97
0.67
0.52
0.33
0.17
0.78
0.35
0.10
0.08
0.15
Negative
Positive
d)
fCO2
fCH4
Temp
Sal
Level
Turb
DO
BP
WSpd
TotPAR
Precip
0.61
1.0
0.25
0.17
0.13
0.63
0.14
0.17
0.13
0.17
0.17
Negative
Positive

Figure 7.

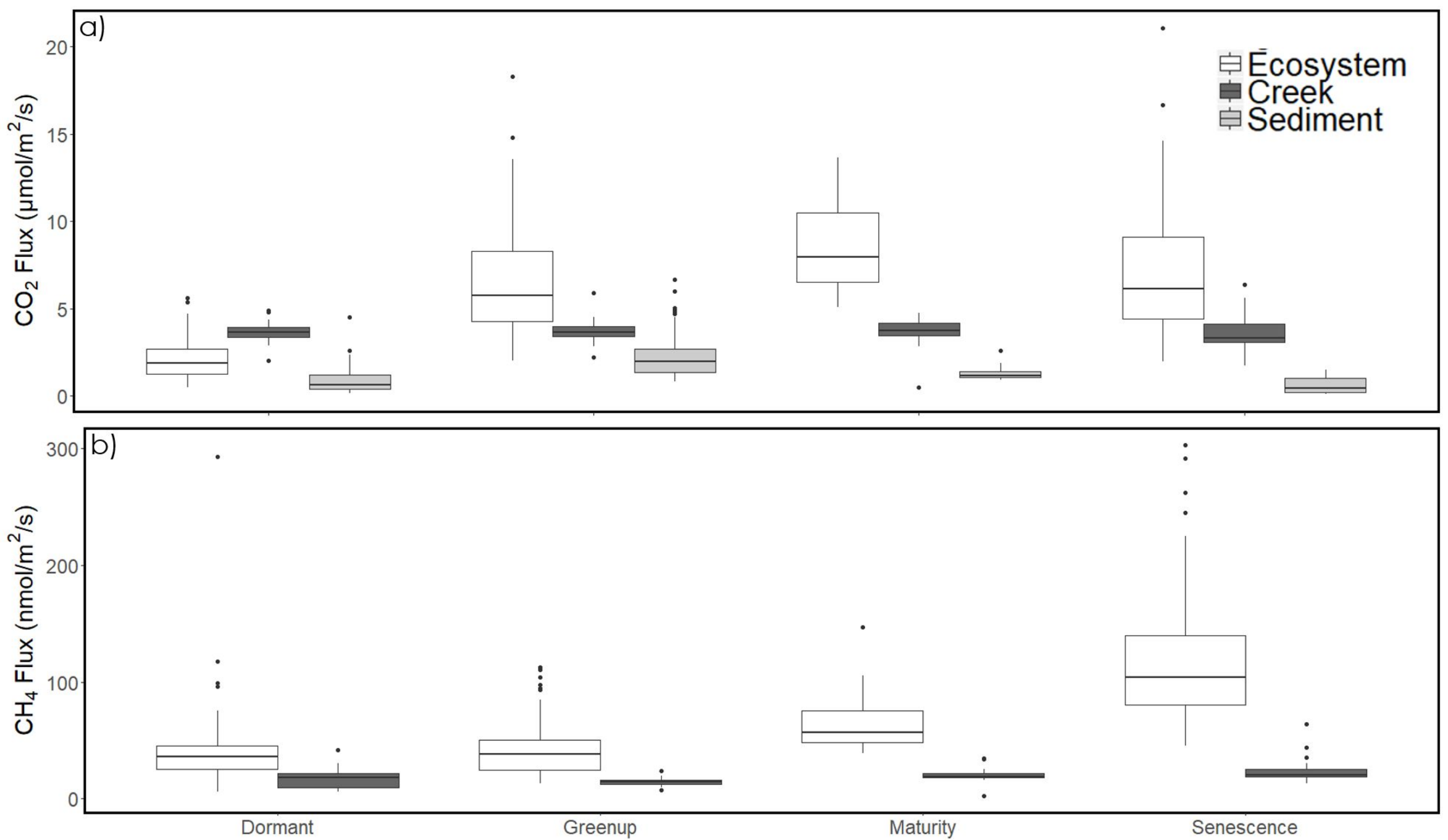
a)
b)
Ecosystem
Creek
Sediment
CO_2 Flux ($\mu mol/m^2/s$)
CH_4 Flux ($nmol/m^2/s$)
0
5
10
15
20
100
200
300
Dormant
Greenup
Maturity
Senescence